# Spin-dependent two-photon Bragg scattering in the Kapitza-Dirac effect

Sven Ahrens,[1,*] Zhenfeng Liang,[1] Tilen Čadež,[2,3,4] and Baifei Shen[1,†]

[1]*Department of Physics, Shanghai Normal University, Shanghai 200234, China*

[2]*Center for Theoretical Physics of Complex Systems, Institute for Basic Science (IBS), Daejeon 34126, Republic of Korea*

[3]*Center of Physics of University of Minho and University of Porto, P-4169-007 Oporto, Portugal*

[4]*CAS Key Laboratory of Theoretical Physics, Institute of Theoretical Physics, Chinese Academy of Sciences, Beijing 100193, China*

(Received 27 January 2020; accepted 4 August 2020; published 9 September 2020)

We present the possibility of spin-dependent Kapitza-Dirac scattering based on a two-photon interaction only. The interaction scheme is inspired from a Compton scattering process, for which we explicitly show the mathematical correspondence to the spin dynamics of an electron diffraction process in a standing light wave. The spin effect has the advantage that it already appears in a Bragg scattering setup with arbitrary low field amplitudes, for which we have estimated the diffraction count rate in a realistic experimental setup at available x-ray free-electron laser facilities.

DOI: 10.1103/PhysRevA.102.033106

## I. INTRODUCTION

The spin is an intrinsic angular momentum of every elementary particle [1]. While from the theoretical point of view one would identify the spin as a byproduct of the quantization procedure of relativistic wave functions, one might in a classical picture imagine the spin as a tiny spinning sphere. This view might be intuitive, but should be considered as technically incorrect. Nevertheless, one is associating a magnetic moment with a magnetic dipole to the electron, which in the classical imagination of a charged, spinning sphere would be the "handle" to interact with the electron spin. More formally, intrinsic angular momentum is characterized by "unitary representations of the inhomogeneous Lorentz group", according to Wigner [2,3]. From the historical perspective, it seems that the electron spin was initially rather an implication from the need for a consistent explanation for the atomic structure, as well as from spectroscopic observations [4], with a first explicit experimental indication from the Stern-Gerlach experiment [5–7].

Within the scientific applications of present times, spin-dependent electron interaction appears commonly in photoemission [8,9], such that interesting applications such as spin- and angle-resolved photoemission spectroscopy (SARPES) [10–12] are possible, with even recording spin-resolved band structure [13–16]. However, these examples have in common that they are bound state systems, in which the electron is not free from interactions with its environment. For isolated electrons, which propagate freely in space, Pauli has already argued in 1932 that an electron interaction with electromagnetic fields cannot be sensitive to the electron spin in terms of a concept of classical trajectories [17]. The reason is that the Stern-Gerlach experiment has been carried out with electrically neutral silver atoms instead of charged electrons. For charged particles, however, the Lorentz force from the magnetic field in the Stern-Gerlach experiment requires a precise knowledge of the electron's initial position and momentum, which is in conflict with the Heisenberg uncertainty relation. Therefore, a common assumption is that "it is impossible, by means of a Stern-Gerlach experiment, to determine the magnetic moment of a free electron" [18] and that "Conventional spin filters, the prototype of which is the Stern-Gerlach magnet, do not work with free electrons" [19]. Nevertheless, proposals for a longitudinal setup of the Stern-Gerlach experiment with electrons exist [20,21], for a "minimum-spreading longitudinal configuration" [22]. Also, random spin flips can be induced by radio-frequency field injection and thermal radiation at an electron in a Penning trap [23,24].

Electron diffraction in standing light waves, as first proposed by Kapitza and Dirac [25] (see, also, [26–31]), could be a way to establish a controlled and explicit spin-dependent interaction of electrons with electromagnetic fields only. A spin-*independent* Kapitza-Dirac effect has already been experimentally demonstrated for atoms [32,33] and also electrons in a strong [34] and weak [35,36] interaction regime. Concerning "strong" and "weak" interaction regimes, we follow a characterization from Batelaan [37,38], where the recoil shift $\epsilon$ (corresponding to the spacing of the kinetic energy of the different electron diffraction orders) is compared to the ponderomotive amplitude $V_0$ of the standing light wave. The system is in the Bragg regime if $\epsilon \gg V_0$ (weak interaction) and in the diffraction regime for $\epsilon \ll V_0$ (strong interaction). Spin effects [39–47] and also spin-dependent diffraction [48–52] (i.e., sorting of electrons according to their spin state) has been discussed theoretically for the Kapitza-Dirac effect. While the original proposal from Kapitza and Dirac considers a two-photon momentum transfer, higher-order photon scattering is possible [41,42,46–49,51–53] but might be suppressed for the case of a weak ponderomotive amplitude of the standing-wave light field in

*ahrens@shnu.edu.cn

†bfshen@shnu.edu.cn

 

the Bragg regime. Therefore, possible implementation difficulties of spin-dependent electron diffraction could arise for the case of a higher number of interacting photons or the necessity to wait for larger fractions of a Rabi cycle of the electron quantum state transition, which could hinder the observation of such higher-order photon interactions. A further discussion about spin-dependent electron diffraction scenarios in laser fields is carried out in the outlook given in Sec. VI at the end of this article. We also point out other theoretical investigations of electron spin dynamics in strong laser fields [54–65], as well as spin-independent electron diffraction scenarios with a controlled phase-space construction [66–70].

In this article, we discuss spin-dependent Kapitza-Dirac diffraction, featuring a two-photon interaction (first feature), which takes place in a Bragg scattering scenario (second feature). In this context, the term "two-photon interaction" means that the electron absorbs and emits one photon in a classical view of the interaction. The second feature, "Bragg scattering scenario", implies that coherent population transfer between the incoming and the diffracted mode allows for the statistical observation of the effect at theoretically arbitrary low field amplitudes. The approach is inspired by a previous work of one of us, which investigated the spin properties in Compton scattering [71]. Accordingly, the effect can be achieved by forming a standing light wave from two counterpropagating laser beams, of which one is linearly polarized and the other is circularly polarized. We then predict the existence of a spin-dependent diffraction effect, if a beam of electrons crosses the standing light wave with a momentum of about $1mc$ along the polarization direction of the linearly polarized laser beam, where $m$ is the electron rest mass and $c$ is the vacuum speed of light.

The article is organized as follows. In Sec. II, we introduce and explain the parameters of our laser-electron scattering scenario. In Sec. III, we define the mathematical framework for the description of the spin-dependent electron diffraction effect and discuss the outcome of an analytic solution in terms of time-dependent perturbation theory. We support these considerations with a relativistic quantum simulation in Sec. IV. After having demonstrated the possibility of this type of two-photon spin-dependent electron diffraction in the Bragg regime, we consider the possibility of an experimental implementation of the effect at the Shanghai High Repetition Rate XFEL and Extreme Light Facility (SHINE) in Sec. V. In the final outlook (Sec. VI), we compare our spin-dependent interaction scheme with other proposals for spin-dependent electron diffraction in the literature. In the appendices, we discuss the perturbative solution of the electron in the standing light wave (Appendix A), a Taylor expansion of the analytic spin-dependent electron scattering formula (Appendix B), a perturbative solution for an interacting, quantized electron-photon system, from which a relation to Compton scattering is established (Appendix C), and expressions of the spin-propagation matrix on the tilted spinor basis, which is used in this article (Appendix D).

## II. CONCEPTUAL REMARKS

As mentioned in Sec. I, we want to demonstrate the discussed spin effect with a parameter setup which corresponds to the scenario in Ref. [71]. Accordingly, we consider electron diffraction at a monochromatic, standing light wave along the $x$ axis,

$$A_\mu(\boldsymbol{x},t)=\tfrac{1}{2}(a_\mu e^{-ik_l\cdot x}+a_\mu^* e^{ik_l\cdot x}+a'_\mu e^{-ik'_l\cdot x}+a'^*_\mu e^{ik'_l\cdot x}). \tag{1}$$

In Eq. (1), we have introduced the two momentum four-vectors of the two counterpropagating laser beams,

$$k_l^\mu=(k_l,\boldsymbol{k}_l),\quad k_l'^\mu=(k_l,-\boldsymbol{k}_l), \tag{2}$$

with wave vector $\boldsymbol{k}_l=k_l\boldsymbol{e}_x$, laser wave number $k_l$, and the two polarizations $a_\mu$ and $a'_\mu$ of the left and right propagating laser beam. Throughout the paper, except for the experimental implementation discussed in Sec. V, we set $c=\hbar=1$, in a Gaussian unit system, such that laser frequency $\omega$ equals the laser wave number $k_l$. The dot between the four-vectors symbolizes a four-vector contraction $k_l\cdot x=k_l^\mu x_\mu$ according to Einstein's sum convention,

$$a_\mu b^\mu=\sum_\mu a_\mu b^\mu, \tag{3}$$

with space-time metric $g_{\mu\nu}=\mathrm{diag}(1,-1,-1,-1)$. Also, we use the symbol $*$ for denoting complex conjugation. The right and left propagating beam is linearly and circularly polarized, respectively and described by the corresponding polarization four-vectors,

$$a=(0,0,0,\mathfrak{A})^{\mathrm{T}},\quad a'=(0,0,\mathfrak{A}',i\mathfrak{A}')^{\mathrm{T}}/\sqrt{2}, \tag{4}$$

where $\mathfrak{A}$ and $\mathfrak{A}'$ are the field amplitudes of the lasers' vector potentials, and T denotes transposition. The electron has the initial momentum

$$\tilde{\boldsymbol{p}}_i=-\boldsymbol{k}_l+m\boldsymbol{e}_z, \tag{5}$$

and we consider the two 45° tilted spin states

$$s^{\searrow}=\begin{pmatrix}\cos 11\pi/8\\ \sin 11\pi/8\end{pmatrix},\quad s^{\nwarrow}=\begin{pmatrix}\cos 15\pi/8\\ \sin 15\pi/8\end{pmatrix} \tag{6}$$

as initial electron spin configurations in this work.

In this following paragraph, we want to give a rough explanation of why the parameters (4)–(6) are taken as they are. Though spin-dependent terms may appear in electron-laser interactions, they are usually dominated by a spin-*independent* term, which can be associated with the ponderomotive potential of the laser beam. Thus, spin dynamics are usually superimposed by pronounced, spin-independent Rabi oscillations [50] which potentially average out the spin effect. However, it is possible that the dominant contribution from the ponderomotive potential can cancel away, for certain configurations of the electron momentum and the laser polarization [42]. It seems that there is a continuum of parameters in parameter space (transverse electron momentum and laser polarizations) for which the spin-preserving terms are suppressed. The discussion about the structure of such a parameter space is beyond the scope of this work, but an investigation which shows a continuous variation of parameters, for which experimentally suitable spin dynamics may appear, is under study. Regarding this article, the related parameters in the follow-up study [71] of Ref. [42] were constructed according to systematic reasoning. Since this specific spin

effect is investigated with particular care in Ref. [71], we prefer to use the parameters in Eqs. (4)–(6) over other possible choices of parameters.

In this context, we would like to point out that Ref. [71] discusses spin dynamics in Compton scattering, whereas in this article, the in- and outgoing photon of the scattering process is substituted by two counterpropagating laser beams. This means that we describe the spin-dependent electron quantum dynamics in an external classical field of the counterpropagating laser-beam background in terms of the Furry picture [72–74]. In the limit of low field amplitudes, however, where processes linear in the external field amplitudes are of relevance only, both described scenarios (Compton scattering and electron diffraction) have identical scattering amplitudes. Note that this association of Compton scattering for electrons in low external fields was already pointed out by Ritus, where the Klein-Nishina formula and also the Breit-Wheeler formula were recovered in the low-field limit of an electron (described by the Dirac equation) in a plane-wave field [75].

The match of Compton scattering and electron diffraction for low fields can be mathematically justified by showing that the perturbative solution of electron quantum dynamics in an external laser field (see Appendix A) can be reformulated into perturbative scattering dynamics of one electron and one photon in the context of an interacting many-particle electron-photon quantum system. This solution of the single electron-photon interaction can, in turn, be cast into the form of the Compton scattering formula (explained in Appendix C 3). We have sketched this lowest-order electron-photon interaction process in the context of virtual particle fluctuations during the interaction in Fig. 1. The four different intermediate particle states that appear, denoted by $\Psi_a$, $\Psi_b$, $\Psi_c$, and $\Psi_d$, can be associated with Figs. 2(a)–2(d), respectively, which can be further summed up to give the two, vertex exchanged contributions of the Feynman graphs [Figs. 2(e) and 2(f)] of Compton scattering. The solutions of time-dependent perturbation theory of a quantized electron-photon system, such as in Fig. 1, are known as old-fashioned perturbation theory (see the literature [3,76]). Beyond the qualitative picture which is discussed in Figs. 1 and 2, we also give a specific calculation in our article, where both perturbative derivations of the processes can be found, in Appendices A and C.

Note that for the computation of the electron dynamics in the two laser beams, we have chosen the monochromatic standing light wave configuration (1) with laser photon momenta (2) because such an arrangement seems to be more common and is also more suitable for a numerical computation. In general, one could also consider bichromatic dynamics or dynamics with nonparallel laser beams. Such a general scenario could, however, then be related by a Lorentz transformation to our described scenario. In the context of the chosen laser photon momenta (2) and the initial electron momentum (5), a nontrivial interaction with each of the laser beams results in the final electron momentum,

$$\tilde{\boldsymbol{p}}_f = \boldsymbol{k}_l + m\boldsymbol{e}_z, \tag{7}$$

as implied by momentum conservation. The longitudinal $x$ component of the initial and final electron momentum is thereby chosen such that energy is also conserved for the electron and photon, which constitute the scattering process in a classical picture.

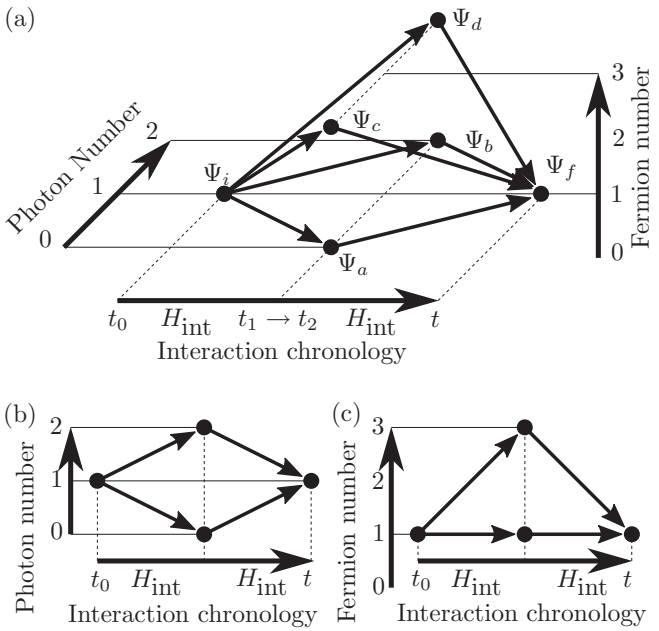


FIG. 1. Particle fluctuations of an interacting photon and electron. (a) When considering the lowest-order interaction of an electron with a photon in a quantized photon-electron description, one encounters the four different particle fluctuation configurations [quantum states in Eqs. (C18)]. In the photonic sector in (b), one either has absorption and then emission of the incoming and outgoing photon, or one first has emission and then absorption of the outgoing and incoming photon. In the electronic sector in (c), one encounters two quantum trajectories, in which either the electron propagates from its initial to its final state or in which the initial electron is accompanied by a virtual electron-positron pair, which then annihilates with the pair's antiparticle, with the final electron state remaining. The pairwise combination of the $2 \times 2$ processes in (b) and (c) gives the four combinations in (a). One can associate these four quantum paths with Feynman graphs, as illustrated in Fig. 2. Note however, that in contrast to the graphical conventions in Fig. 2 which correspond to Feynman graphs, the roles of vertices and arrows are interchanged in the graphical representation in this figure: The big black dot corresponds to the free propagation of the quantum state, whereas the arrows indicate a change of the quantum state which is caused by the interaction $H_{\rm int}$. See Appendix C for more information.

## III. THEORETICAL DESCRIPTION

The electron quantum dynamics is computed by making a plane-wave decomposition of the electron wave function,

$$\psi(\boldsymbol{x}, t) = \sum_{n,s} \left[ c_n^s(t) u_{\boldsymbol{k}_n}^s e^{-i\boldsymbol{k}_n \cdot \boldsymbol{x}} + d_n^s(t) v_{-\boldsymbol{k}_n}^s e^{-i\boldsymbol{k}_n \cdot \boldsymbol{x}} \right]. \tag{8}$$

The approach allows for the transfer of multiple photon momenta $\boldsymbol{k}_n = \boldsymbol{p}_i + n\boldsymbol{k}_L$, with the partial wave's complex amplitudes $c_n^s(t)$, $d_n^s(t)$ for positive and negative solutions,

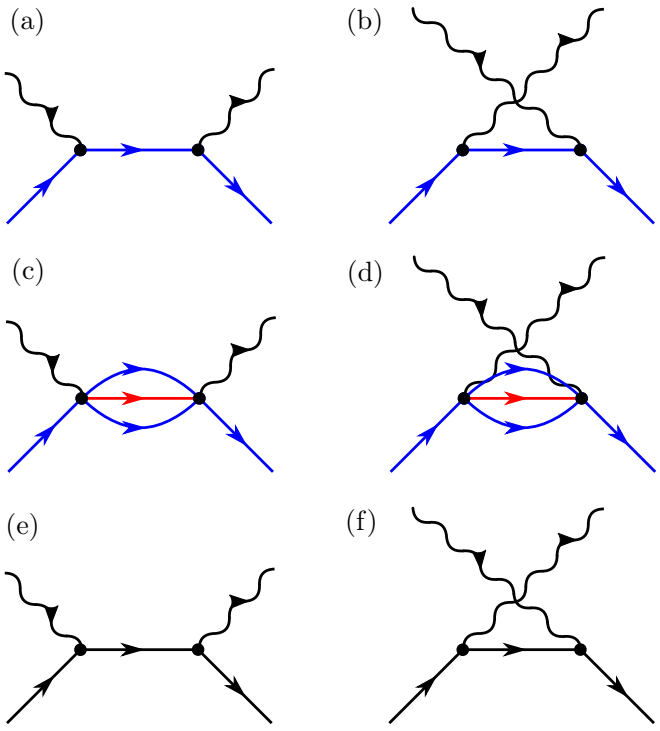


FIG. 2. Association of Feynman graphs with a corresponding split-up version of the electron propagator. One can show that the four quantum paths in Fig. 1 with $\Psi_a$, $\Psi_b$, $\Psi_c$, and $\Psi_d$ sketched in (a)–(d), respectively, can be combined into the Feynman graphs (e) and (f). More precisely, (e) is composed of the processes in (a) and (c), and (f) is composed of the processes in (b) and (d). The corresponding mathematical identification is carried out in Appendix C 3.

respectively. The positive and negative solutions of the free Dirac equation are the bispinors,

$$u_{\boldsymbol{k}}^{s} = \sqrt{\frac{m}{\mathcal{E}_{\boldsymbol{k}}}}\sqrt{\frac{\mathcal{E}_{\boldsymbol{k}}+m}{2m}}\begin{pmatrix}\chi^{s}\\ \frac{\boldsymbol{\sigma}\cdot\boldsymbol{k}}{\mathcal{E}_{\boldsymbol{k}}+m}\chi^{s}\end{pmatrix}, \tag{9a}$$

$$v_{\boldsymbol{k}}^{s} = \sqrt{\frac{m}{\mathcal{E}_{\boldsymbol{k}}}}\sqrt{\frac{\mathcal{E}_{\boldsymbol{k}}+m}{2m}}\begin{pmatrix}\frac{\boldsymbol{\sigma}\cdot\boldsymbol{k}}{\mathcal{E}_{\boldsymbol{k}}+m}\chi^{s}\\ \chi^{s}\end{pmatrix}, \tag{9b}$$

where $s$ denotes the spin of each wave. The $\boldsymbol{p}_i$ is the initial electron momentum, whose transverse component can differ from Eq. (5) at the stage of derivation, and $\mathcal{E}_{\boldsymbol{k}} = \sqrt{m^2+\boldsymbol{k}^2}$ is the relativistic energy momentum relation of the electron. The vector $\boldsymbol{\sigma}$ is the vector $(\sigma_1,\sigma_2,\sigma_3)^{\mathrm{T}}$ of the Pauli matrices

$$\sigma_x = \begin{pmatrix}0&1\\1&0\end{pmatrix},\quad \sigma_y = \begin{pmatrix}0&-i\\i&0\end{pmatrix},\quad \sigma_z = \begin{pmatrix}1&0\\0&-1\end{pmatrix}, \tag{10}$$

where we use the indices $\{1,2,3\}$ and $\{x,y,z\}$ interchangeably for indexing Pauli matrices in this article. The dot between the three-component spacial vectors in Eq. (8) denotes the inner product in Euclidean space, $\boldsymbol{k}_n\cdot\boldsymbol{x} = \sum_a \boldsymbol{k}_{n,a}x_a$. The two-component objects $\chi^s = (\chi_1^s,\chi_2^s)^{\mathrm{T}}$ denote spinors. Note that in Refs. [42,50] the bispinors $v_{\boldsymbol{k}}^s$ [see Eq. (9b)] have been introduced with opposite momentum $\boldsymbol{k}$. We also point out that we have absorbed the phase-space factor $(m/\mathcal{E}_{\boldsymbol{k}})^{1/2}$ from the Compton cross-section formula into the normalization of the spinor definition (9). Furthermore, we mention that the form of the wave function's plane-wave expansion in Eq. (8) is an implication from the standing light wave (1).

The time evolution of the wave function (8) in terms of its expansion coefficients can be formally written as

$$c_n^s(t) = \sum_{a,s'}\left[U_{n,a}^{+,s;+,s'}(t,0)c_a^{s'}(0) + U_{n,a}^{+,s;-,s'}(t,0)d_a^{s'}(0)\right],$$

$$d_n^s(t) = \sum_{a,s'}\left[U_{n,a}^{-,s;+,s'}(t,0)c_a^{s'}(0) + U_{n,a}^{-,s;-,s'}(t,0)d_a^{s'}(0)\right]. \tag{11}$$

A perturbative expression of the propagation functions $U_{n,a}^{\gamma,s;\gamma',s'}(t,0)$ can be provided by transforming the Dirac equation,

$$i\dot{\psi}(\boldsymbol{x},t) = \{[-i\boldsymbol{\nabla} - \mathrm{e}\boldsymbol{A}(\boldsymbol{x},t)]\cdot\boldsymbol{\alpha} + m\beta + \mathrm{e}A^0(\boldsymbol{x},t)\}\psi(\boldsymbol{x},t), \tag{12}$$

into momentum space and applying second-order time-dependent perturbation theory to the resulting equations of motion. In Eq. (12), the $\boldsymbol{\alpha}$ and $\beta$ are the Dirac matrices

$$\alpha_i = \begin{pmatrix}0&\sigma_i\\\sigma_i&0\end{pmatrix},\quad \beta = \begin{pmatrix}\mathbb{1}&0\\0&-\mathbb{1}\end{pmatrix}, \tag{13}$$

where $\mathbb{1}$ is the $2\times 2$ identity matrix. The elementary electric charge e simplifies into the square root of the fine-structure constant $\mathrm{e} = \sqrt{\alpha}$ in our chosen unit system. The dot on top of the wave function $\psi(\boldsymbol{x},t)$ in Eq. (12) denotes its time derivative $\dot{\psi}(\boldsymbol{x},t) = \partial\psi(\boldsymbol{x},t)/\partial t$. The procedure of rewriting and perturbatively solving the Dirac equation in a momentum-space description is similar to the corresponding procedures in Refs. [42,44]. Therefore, we have shifted the details of the calculation to Appendix A and focus on the physics description here.

The perturbative solution of the spin-dependent quantum state propagation of the initial electron spin state $c_0(0)$ to the final electron spin state $c_2(0)$ is proportional to the matrix

$$M_s = \frac{1}{\sqrt{8}}\begin{pmatrix}-1&-1-\sqrt{2}\\-1+\sqrt{2}&1\end{pmatrix} = s^{\nwarrow}\cdot s^{\searrow\dagger}, \tag{14}$$

for our chosen parameters of the photon polarization (4) and the initial electron momentum (5). We take this spin-propagation matrix from the Taylor expansion of the spin-propagation matrix $M$ in Appendix B. In this context, we point out that we desire that spin-preserving terms (terms proportional to $\mathbb{1}$) cancel in the electron spin dynamics, as mentioned above. This is approximately the case for the transverse momenta of $\tilde{\boldsymbol{p}}_i$ in Eq. (5). However, small corrections remain, such that we choose

$$(\tilde{\boldsymbol{p}}_i)_3 \approx (1+1.34\ldots\times 10^{-4})m \tag{15}$$

for the $z$ component of the electron momentum in our numerical simulation with the selected laser photon energy of $k_l = 13\ \mathrm{keV} = 0.025\ldots m$. Nevertheless, the corrections to $\tilde{\boldsymbol{p}}_i$ are more than two orders of magnitude smaller than the photon momentum $k_l$ itself, such that the correction (15) has no strong influence on the physics which is discussed in this work.

The right-hand side of Eq. (14) shows an outer product representation of $M_s$, created from the pair of two-component spinors $s^{\searrow}$ and $s^{\searrow}$. This can be seen from their expressions,

$$s^{\searrow} = \begin{pmatrix} 1-\sqrt{2} \\ -1 \end{pmatrix} \sqrt{2(2-\sqrt{2})}^{-1}, \tag{16a}$$

$$s^{\nwarrow} = \begin{pmatrix} 1+\sqrt{2} \\ -1 \end{pmatrix} \sqrt{2(2+\sqrt{2})}^{-1}, \tag{16b}$$

which are equivalent to the definitions (6) and consistent with the convention in Ref. [71]. From the outer product representation of the matrix $M_s$ at the right-hand side of Eq. (14), one immediately obtains

$$\langle s^{\searrow}|M_s|s^{\searrow}\rangle = 0, \quad \langle s^{\nwarrow}|M_s|s^{\searrow}\rangle = 1, \tag{17a}$$

$$\langle s^{\searrow}|M_s|s^{\nwarrow}\rangle = 0, \quad \langle s^{\nwarrow}|M_s|s^{\nwarrow}\rangle = 0, \tag{17b}$$

which is consistent with the corresponding scenario in Compton scattering [71], where a $s^{\searrow}$-polarized electron is scattered at a vertically polarized photon into a left circularly polarized photon and a $s^{\nwarrow}$-polarized electron. The opposite scenario, where a $s^{\nwarrow}$-polarized electron is scattered into a right circularly polarized photon and a $s^{\searrow}$-polarized electron (see Ref. [71]) is considered to be overruled by the effect of induced emission into a left circularly polarized photon, for the case of coherent electron diffraction with the laser polarization (4) in the Kapitza-Dirac scattering.

## IV. NUMERICAL SOLUTION OF THE SPIN-DEPENDENT QUANTUM DYNAMICS

We support the above considerations by performing numerical simulations of the one-particle Dirac equation in momentum space (A1) [i.e., a numerical solution of the propagation equation (11)] of an electron in a standing wave of light in Fig. 3. Such a procedure is similar to the numerical simulations shown in Refs. [41–45,47,49–51]. In the simulation, the standing wave of light (1) has the polarization (4). The standing wave's field amplitude is smoothly ramped up and down for the duration of five laser periods at the beginning and the end of the simulation by a $\sin^2$ temporal envelope, as done in Refs. [41–45,47,49–51].

In the numerical simulation, we see no diffraction dynamics for an electron with initial $s^{\nwarrow}$ spin configuration, i.e., we have

$$|\langle s^{\nwarrow}\,|\,U_{0,0}^{+;+}(t,0)\,|\,s^{\nwarrow}\rangle|^2 \approx 1, \tag{18a}$$

$$|\langle s^{\searrow}\,|\,U_{0,0}^{+;+}(t,0)\,|\,s^{\nwarrow}\rangle|^2 \approx 0, \tag{18b}$$

$$|\langle s^{\nwarrow}\,|\,U_{2,0}^{+;+}(t,0)\,|\,s^{\nwarrow}\rangle|^2 \approx 0, \tag{18c}$$

$$|\langle s^{\searrow}\,|\,U_{2,0}^{+;+}(t,0)\,|\,s^{\nwarrow}\rangle|^2 \approx 0. \tag{18d}$$

This is consistent with our analytic considerations from perturbation theory; see Eq. (17b). For this reason, we only show the projection on the diffracted spin state,

$$|\langle s^{\nwarrow}\,|\,U_{2,0}^{+;+}(t,0)\,|\,s^{\searrow}\rangle|^2, \tag{19a}$$

and the initial quantum state,

$$|\langle s^{\searrow}\,|\,U_{0,0}^{+;+}(t,0)\,|\,s^{\searrow}\rangle|^2, \tag{19b}$$

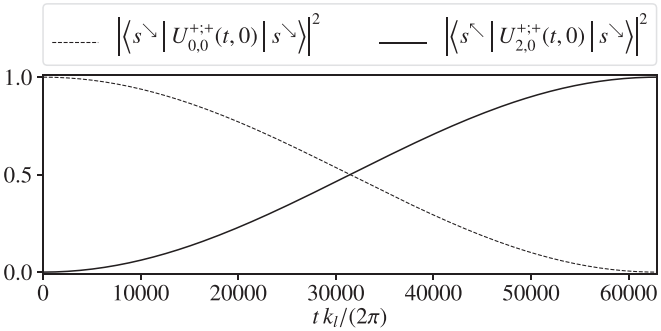


FIG. 3. Simulated spin-dependent electron diffraction effect. The panel shows the two nonvanishing matrix elements of the numerical solution of the Dirac equation in momentum space (A1), represented by the quantum state propagation (11). The simulation is carried out with the field amplitudes $\mathfrak{A}$ and $\mathfrak{A}'$ and laser photon energy $k_l$ as specified in Eq. (24), where the initial electron momentum is $\tilde{\boldsymbol{p}}_i$ [see Eq. (5)]. One can see that the system follows the simple Rabi model (21), from an electron with initial momentum $k_0$ and spin state $s^{\searrow}$ into an electron with final momentum $k_2$ and spin state $s^{\nwarrow}$. For the opposite initial spin configuration $s^{\nwarrow}$, we find that no such Rabi oscillations occur, which demonstrates a theoretically perfect spin-filtering and spin-polarization effect.

of the numerical solution of the propagation $U_{a,b}^{+,+}(t,0)$ in Fig. 3. In fact, these are the only non-negligible contributions of the time evolution. Equivalently, one can say that both expressions (19) sum up to approximately 1, such that the unitarity of the Dirac equation implies that any other excitations are negligibly small.

Note that the half-period Rabi cycle, which is shown in Fig. 3, lasts for $6.29 \times 10^4$ optical cycles of the laser field, corresponding to the Rabi frequency

$$\Omega_R = 2.02 \times 10^{-7} m \tag{20}$$

in the effective Rabi model,

$$|\langle s^{\nwarrow}\,|\,U_{2,0}^{+;+}(t,0)\,|\,s^{\searrow}\rangle|^2 = \sin\left(\frac{\Omega_R t}{2}\right)^2. \tag{21}$$

This is consistent with the approximate equation for the matrix element,

$$|\langle s^{\nwarrow}\,|\,U_{2,0}^{+;+}(t,0)\,|\,s^{\searrow}\rangle|^2 \approx \left(\frac{\mathrm{e}\mathfrak{A}\mathrm{e}\mathfrak{A}' k_l t}{8m^2\sqrt{2}}\right)^2, \tag{22}$$

of the perturbative solution of the Dirac equation in Eq. (B2). In this context, we assume that the left-hand side of Eq. (22) can be identified with the analytic short-time approximation of the Rabi model (21),

$$|\langle s^{\nwarrow}\,|\,U_{2,0}^{+;+}(t,0)\,|\,s^{\searrow}\rangle|^2 \approx \left(\frac{\Omega_R t}{2}\right)^2, \tag{23}$$

where we have set the parameters

$$\mathrm{e}\mathfrak{A}/m = \mathrm{e}\mathfrak{A}'/m = 4.74 \times 10^{-2}, \tag{24a}$$

$$k_l/m = 2.54 \times 10^{-2}, \tag{24b}$$

in our numerical simulation. We choose the photon energy to be 13 keV, corresponding to the value of $k_l$ in Eq. (24b) for the simulation. Similarly, we have set the simulation's laser-field

amplitude $\mathfrak{A}$ and $\mathfrak{A}'$ in (24a) such that a half Rabi period will last exactly 20 fs. This value corresponds to the value of the Rabi frequency (20).

The actual numerical implementation was carried out in the basis of the states $c_n^s$ and $d_n^s$ with spin-up and spin-down $s \in \{\uparrow, \downarrow\}$, where the matrix elements with respect to the spin states $s^{\searrow}$ and $s^{\nwarrow}$ of the numerical propagation $U_{a,b}^{+,+}(t,0)$ are given explicitly in Appendix D. Note that the transition amplitudes $U_{n,0}(t,0)$ of higher momentum states $|n|$ are dropping off exponentially for the chosen parameters in Eq. (24), such that we have truncated the higher modes in the numerical solutions at $|n| = 12$, similar to the procedure in Refs. [41–45,47,49–51].

We want to point out that Eqs. (17) demonstrate a spin-dependent diffraction effect: While the initial spin configuration $s^{\searrow}$ is diffracted into a $s^{\nwarrow}$ configuration, an initial spin $s^{\nwarrow}$ is not diffracted *at all*. Thus, electrons are filtered according to their initial spin orientation. Also, the outer product in (14) implies that whatever electron spin is diffracted, the final electron spin will always be $s^{\nwarrow}$. This also demonstrates that the electron spin can be polarized by the diffraction mechanism. These two properties (filtering and polarization of the electron spin) are the same characterizations which we have already pointed out in our previous work [50], where a two-photon spin-dependent diffraction is presented which has similar properties as in this work. However, the spin-dependent diffraction effect in Ref. [50] only appears after multiple Rabi cycles, whereas the spin-dependent diffraction in our current work already appears with the rise of the transition's oscillation in the form of a Bragg peak, which appears to be more suitable for the experimental implementation.

We also want to point out that the spin-dependent propagation matrix in Eq. (14) is a generalization of our statement in Ref. [50], in which a spin-dependent quantum state propagation has been identified to be proportional to a projection matrix. In contrast, Eq. (14) explicitly demonstrates that even a projection is not the most general characterization for spin-dependent dynamics. A general and specific criterion for spin-dependent diffraction dynamics might be nontrivial and be a subject of future investigations.

## V. EXPERIMENTAL IMPLEMENTATION CONSIDERATIONS

We want to discuss a possible experimental implementation of the spin-dependent laser-electron interaction, according to the setup in Fig. 4. In this example, the source of the x-ray laser beams is assumed to be the Shanghai High Repetition Rate XFEL and Extreme Light Facility (SHINE), which is currently under construction [77]. Within its design parameters, SHINE will provide 100 GW laser pules at 13 keV photon energy and with a pulse duration of 20 fs. When the beam is focused to 100 nm, the peak intensity reaches $1.2 \times 10^{21}$ W/cm$^2$. A coincident laser pulse overlap at the interaction point is achieved by reflecting the two beams as in the arrangement in Fig. 4. Circular polarization can be converted from the linear polarized laser beam by utilizing a phase-retardation setup in x-ray diffraction [78]. In this way, two coincident, counterpropagating, high-intensity pulses can be established at the beam focus, with a linearly polarized

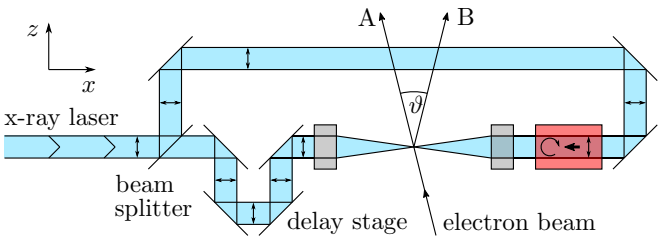


FIG. 4. Possible experimental setup for establishing spin-dependent electron diffraction based on two-photon Kapitza-Dirac scattering. A linearly polarized x-ray laser with 13 keV photon energy is entering from the left. A part of the beam is transmitted through the beam splitter and the reflected part of the x-ray laser beam is guided to approach the beam focus from the opposite direction. A phase retarder (red box with an opened arrow circle) is converting the linear x-ray polarization into circular polarization. All x-ray optics are chosen such that the two counterpropagating laser beams are reaching the beam focus with equal intensity and at equal time. For the setup, spin-dependent diffraction is expected to be observed for initially spin-polarized electrons, which approach the laser focal spot with a kinetic energy of 212 keV at an inclination angle $90^\circ - \vartheta/2$ to the beam propagation direction (see main text for details). The small gray rectangular boxes symbolize the beam focusing optics.

beam from the left and a circularly polarized beam from the right. By assuming mirror reflectivities of 85%, a phase-retarder transmittivity of 55% and a beam-splitter design with 34% transmission and 56% reflection [79], one estimates an intensity of $1.2 \times 10^{20}$ W/cm$^2$ for the left and right beams at the laser focus spot. Equation (22) can be written in terms of SI units as

$$|\langle s^{\nwarrow}|\, U_{2,0}^{+;+}(t,0)\,|\, s^{\searrow}\rangle|^2 \approx \left(\frac{\alpha\lambda_c^2}{8\pi\sqrt{2}}\frac{I_1^{1/2}I_2^{1/2}t}{c\hbar k_l}\right)^2. \qquad (25)$$

Here, $\alpha$ is the fine-structure constant, $\lambda_c$ is the Compton wavelength, and $I_1$ and $I_2$ are the intensities of the left- and right-propagating laser beams, respectively. Evaluated with the parameters above, one is expecting a probability of about $1.1 \times 10^{-7}$ for an electron with a spin-$\searrow$ orientation to be diffracted in the direction of beam $B$. Since we are discussing a spin-dependent diffraction scheme, electrons with spin-$\nwarrow$ orientation will not be diffracted into beam $B$. For undergoing spin-dependent diffraction, the electrons must have the specific momentum of 511 keV/$c$ along the $z$ axis, corresponding to a kinetic energy 212 keV. When undergoing diffraction, the electron will pick up two longitudinal photon momenta of 13 keV/$c$ along the $x$ axis. Since the momentum change is longitudinal, one can relate this to a diffraction angle of $\vartheta = 2.9^\circ$ from the scattering geometry. Spin-polarized electron pulses with charges of 10 fC are available [80] and, with the temporal electron bunch width of 10 ps, one expects 124 electrons to cross the beam focal spot in its 20 fs duration. Therefore, with the SHINE aimed repetition rate of 1 MHz, we estimate a count rate of 13 electrons per second for the spin-dependent electron diffraction effect. Similar parameters for establishing the considered experimental configuration can also be reached at the Linac Coherent Light Source in

Stanford, CA [81] and the European X-FEL in Hamburg, Germany [82].

## VI. DISCUSSION AND OUTLOOK

In this article, we have discussed a spin-dependent Kapitza-Dirac diffraction effect, which can be implemented in the form of a Bragg scattering setup and which requires only the interaction with two of the standing light wave's photons. Open questions for the effect are the influence of the laser-beam focus on the spin-dependent electron dynamics. Within this article, we have treated the laser beam and also the electron wave function as a discrete superposition of a finite number of plane waves, whereas a Gaussian beam and a Gaussian wave packet would model the electron and laser more realistically. In this context, the question arises as to how a small longitudinal field component [83], which is implied by the laser-beam focus, is influencing the spin dynamics. Also, the contribution of spontaneous emission of electromagnetic radiation compared to the induced emission into the laser beam is of relevance and can be computed [84]. The question of how the quantum state of the laser field is modified by the electron diffraction dynamics is also of relevance because the Compton scattering version of the effect raises questions about the transfer of intrinsic angular momentum (spin) between the electron and the photon [71].

There are two possible laser-frequency regimes for the implementation of the effect, which are realistic in terms of the available laser intensity for the experiment: the optical regime and the x-ray regime.

The optical regime has the advantage that the classical nonlinearity parameter $\xi = \mathrm{e}\mathfrak{A}/m$ can reach values of 1 with comparably low effort, such that high-photon-number Kapitza-Dirac scattering, as, for example, discussed in Refs. [41,42,46–49,51–53], could be possible. Note that the short-time diffraction probability and the transition's Rabi frequency are proportional to the field amplitude $\mathfrak{A}$ to the power of the number of interacting photons, implying that either $\xi$ should be close to 1 or the number of contributing photons should be as small as possible. Bichromatic setups [49,51] appear promising for the experiment due to potentially long laser-electron interaction times caused by low initial and final electron momenta. However, one challenge with optical systems would be the control of the transverse electron momentum and the laser polarization such that the effect does not smear out. A look at the matrix (B5) of the polarization-dependent spin dynamics for the electron in the laser beam tells us that the electron momentum should be under control on the order of the photon momentum $k_l$. Also, the laser polarization should be controlled on the accuracy level $k_l/m$, where we have $k_l \approx 10^{-6} m$ in the optical regime.

In the x-ray regime, on the other hand, this need for fine tuning would only be at the percent level. Here, one faces the challenge of providing field amplitudes, such that $\xi$ is close to one, which might be possible for the case of small beam foci. Therefore, for implementing a spin-dependent diffraction setup for x rays, a lower-order photon interaction Kapitza-Dirac effect would be beneficial. Two-photon scattering would be the lowest possible configuration for Kapitza-Dirac-like scattering since a one-photon interaction is not compatible with the conservation of energy and momentum. A two-photon setup from a previous investigation, which only depends on a longitudinal electron momentum [45,50], appears to be promising. However, for this scenario, one faces the challenge that the spin oscillations are dependent on simultaneous Rabi oscillations with an enhanced frequency by the factor $m/k_l$, which also would imply the necessity of fine tuning. In contrast, the spin-dependent two-photon effect, which is discussed within this article, is *not* superimposed by a larger spin-preserving term in the electron spin propagation. Therefore, only the beginning of a Rabi cycle (i.e., the Bragg peak) of the diffraction effect would have to be observed for seeing the spin-dependent electron-laser interaction. For this reason, the spin-dependent electron diffraction effect, as discussed in Sec. V, appears to be suitable for implementing spin-dependent electron diffraction in standing light waves.

## ACKNOWLEDGMENTS

S.A. thanks C. Müller and C.-P. Sun for discussions. This work has been supported by the National Science Foundation of China (Grants No. 11975155 and No. 1935008) and the Ministry of Science and Technology of the People's Republic of China (Grants No. 2018YFA0404803 and No. 2016YFA0401102). T.Č. gratefully acknowledges the support by the Institute for Basic Science in Korea (Project No. IBS-R024-D1).

## APPENDIX A: PERTURBATIVE SOLUTION OF THE DIRAC EQUATION IN AN EXTERNAL STANDING LIGHT WAVE

In this Appendix, we carry out a perturbative electron spin-dynamics calculation, which is used in Sec. III. As mentioned, according to a similar procedure in Refs. [42,44,50], the Dirac equation (12) can be rewritten into a momentum-space description with respect to the wave-function ansatz (1) by projecting the plane-wave eigensolutions $u^s_{\boldsymbol{k}_n} e^{-i\boldsymbol{k}_n\cdot\boldsymbol{x}}$ and $v^s_{-\boldsymbol{k}_n} e^{-i\boldsymbol{k}_n\cdot\boldsymbol{x}}$ of the Dirac equation from the left. This results in the coupled system of differential equations,

$$\begin{aligned} i\dot{c}^s_n(t) &= \mathcal{E}_{\boldsymbol{k}_n} c^s_n(t) + \sum_{n',s'} \big[V^{+,s;+,s'}_{n,n'}(t) c^{s'}_{n'}(t) \\ &\quad + V^{+,s;-,s'}_{n,n'}(t) d^{s'}_{n'}(t)\big], \qquad \text{(A1a)} \\ i\dot{d}^s_n(t) &= -\mathcal{E}_{\boldsymbol{k}_n} d^s_n(t) + \sum_{n',s'} \big[V^{-,s;+,s'}_{n,n'}(t) c^{s'}_{n'}(t) \\ &\quad + V^{-,s;-,s'}_{n,n'}(t) d^{s'}_{n'}(t)\big], \qquad \text{(A1b)} \end{aligned}$$

where the potential interaction functions $V^{\gamma,s;\gamma',s'}_{n,n'}(t)$ are related to the standing light wave's potential (1) by

$$\begin{aligned} V^{\gamma,s;\gamma',s'}_{n,n'}(t) &= -\frac{\mathrm{e}}{2} L^{\gamma,s;\gamma',s';\mu}_{n,n'} \\ &\quad \times [(a_\mu e^{-ik_l t} + a'^{*}_\mu e^{ik_l t})\delta_{n',n+1} \\ &\quad + (a^*_\mu e^{ik_l t} + a'_\mu e^{-ik_l t})\delta_{n',n-1}]. \qquad \text{(A2)} \end{aligned}$$

Here, we have introduced the additional expressions

$$L^{+,s;+,s';\mu}_{n,n'} = u^{s\dagger}_{\boldsymbol{k}_n}\gamma^0\gamma^\mu u^{s'}_{\boldsymbol{k}_{n'}}, \tag{A3a}$$
$$L^{+,s;-,s';\mu}_{n,n'} = u^{s\dagger}_{\boldsymbol{k}_n}\gamma^0\gamma^\mu v^{s'}_{-\boldsymbol{k}_{n'}}, \tag{A3b}$$
$$L^{-,s;+,s';\mu}_{n,n'} = v^{s\dagger}_{-\boldsymbol{k}_n}\gamma^0\gamma^\mu u^{s'}_{\boldsymbol{k}_{n'}}, \tag{A3c}$$
$$L^{-,s;-,s';\mu}_{n,n'} = v^{s\dagger}_{-\boldsymbol{k}_n}\gamma^0\gamma^\mu v^{s'}_{-\boldsymbol{k}_{n'}}, \tag{A3d}$$

as generalized spin- and polarization-dependent coupling terms, where $\gamma^0 = \beta$ and $\gamma^i = \beta\alpha_i$ are the Dirac gamma matrices. The dagger symbol † denotes combined complex conjugation and transposition.

One can establish a second-order perturbative approximation of the quantum state propagation (11) by (see, for example, [85])

$$U(t,t_0) \approx \frac{1}{i^2}\int_{t_0}^{t} dt_2 \int_{t_0}^{t_2} dt_1 \times U_0(t,t_2)V(t_2)U_0(t_2,t_1)V(t_1)U_0(t_1,t_0), \tag{A4}$$

where $U$ and $V$ are matrices with the matrix product

$$[U_0(t_2,t_1)V(t_1)]^{\gamma,s;\gamma'',s''}_{n,n''} = \sum_{n',\gamma',s'} U^{\gamma,s;\gamma',s'}_{0;n,n'}(t_2,t_1)V^{\gamma',s';\gamma'',s''}_{n',n''}(t_1). \tag{A5}$$

The perturbative propagator (A4) makes use of the expressions $U_0(t,t_0)$, which denote the free propagation,

$$U^{+,s;+,s'}_{0;n,n'}(t,t_0) = \exp[-i\mathcal{E}_{\boldsymbol{k}_n}(t-t_0)]\delta_{n,n'}\delta_{s,s'}, \tag{A6a}$$
$$U^{-,s;-,s'}_{0;n,n'}(t,t_0) = \exp[i\mathcal{E}_{\boldsymbol{k}_n}(t-t_0)]\delta_{n,n'}\delta_{s,s'}, \tag{A6b}$$
$$U^{+,s;-,s'}_{0;n,n'}(t,t_0) = U^{-,s;+,s'}_{n,n'}(t,t_0) = 0, \tag{A6c}$$

for the momentum-space expansion coefficients $c^s_n$ and $d^s_n$. In Secs. II and III, we have introduced the setup of the electron and the standing light wave, such that the electron with initial momentum $\boldsymbol{k}_0$ can be scattered into the final momentum state $\boldsymbol{k}_2$, and such that energy is conserved for the electron and the interacting photons. Interaction terms, which result in this final momentum $\boldsymbol{k}_2$, will grow linear in time in the perturbative expression (A4) and can dominate other contributions. Such a linear growth leads to Rabi oscillations, if one would account for all higher perturbation orders, as implied by the unitary time evolution (see Ref. [27] and Fig. 3). By only accounting for the mentioned resonant terms, we obtain

$$U^{+,s';+,s}_{2,0}(t,t_0) \approx \frac{\mathrm{e}^2 a'^{*}_{\mu} a_\nu}{4i^2}\sum_{s''}\int_{t_0}^{t} dt_2 \int_{t_0}^{t_2} dt_1 \tag{A7a}$$
$$\times \Big\{L^{+,s';+,s'';\mu}_{2,1} L^{+,s'';+,s;\nu}_{1,0}\xi_a(t,t_2,t_1,t_0) \tag{A7b}$$
$$+ L^{+,s';+,s'';\nu}_{2,1} L^{+,s'';+,s;\mu}_{1,0}\xi_b(t,t_2,t_1,t_0) \tag{A7c}$$
$$+ L^{+,s';-,s'';\nu}_{2,1} L^{-,s'';+,s;\mu}_{1,0}\xi_c(t,t_2,t_1,t_0) \tag{A7d}$$
$$+ L^{+,s';-,s'';\mu}_{2,1} L^{-,s'';+,s;\nu}_{1,0}\xi_d(t,t_2,t_1,t_0)\Big\}, \tag{A7e}$$

with the phases

$$\xi_a = \exp[-i\mathcal{E}_{\boldsymbol{k}_2}t + i\big(\mathcal{E}_{\boldsymbol{k}_0} - \mathcal{E}_{\boldsymbol{k}_1} + k_l\big)(t_2-t_1) + i\mathcal{E}_{\boldsymbol{k}_0}t_0],$$
$$\xi_b = \exp[-i\mathcal{E}_{\boldsymbol{k}_2}t + i\big(\mathcal{E}_{\boldsymbol{k}_0} - \mathcal{E}_{\boldsymbol{k}_1} - k_l\big)(t_2-t_1) + i\mathcal{E}_{\boldsymbol{k}_0}t_0],$$
$$\xi_c = \exp[-i\mathcal{E}_{\boldsymbol{k}_2}t + i\big(\mathcal{E}_{\boldsymbol{k}_0} + \mathcal{E}_{\boldsymbol{k}_1} - k_l\big)(t_2-t_1) + i\mathcal{E}_{\boldsymbol{k}_0}t_0],$$
$$\xi_d = \exp[-i\mathcal{E}_{\boldsymbol{k}_2}t + i\big(\mathcal{E}_{\boldsymbol{k}_0} + \mathcal{E}_{\boldsymbol{k}_1} + k_l\big)(t_2-t_1) + i\mathcal{E}_{\boldsymbol{k}_0}t_0], \tag{A8}$$

where the argument $(t,t_2,t_1,t_0)$ is left away at the left-hand side of Eqs. (A8). We made use of $\mathcal{E}_{\boldsymbol{k}_2} = \mathcal{E}_{\boldsymbol{k}_0}$ in Eqs. (A8), as implied by energy conservation. The phase terms

$$+i\big(\mathcal{E}_{\boldsymbol{k}_0} - \mathcal{E}_{\boldsymbol{k}_1} + k_l\big)(t_2-t_1), \tag{A9a}$$
$$+i\big(\mathcal{E}_{\boldsymbol{k}_0} - \mathcal{E}_{\boldsymbol{k}_1} - k_l\big)(t_2-t_1), \tag{A9b}$$
$$+i\big(\mathcal{E}_{\boldsymbol{k}_0} + \mathcal{E}_{\boldsymbol{k}_1} - k_l\big)(t_2-t_1), \tag{A9c}$$
$$+i\big(\mathcal{E}_{\boldsymbol{k}_0} + \mathcal{E}_{\boldsymbol{k}_1} + k_l\big)(t_2-t_1) \tag{A9d}$$

produce the mentioned linear growth behavior in the integral over $t_2$, for the upper limit of the $t_1$ integration, such that we obtain

$$U^{+,s';+,s}_{2,0}(t,t_0) \tag{A10a}$$
$$\approx -i\frac{\mathrm{e}^2 a'^{*}_{\mu} a_\nu}{4}(t-t_0)\exp\big[-i\mathcal{E}_{\boldsymbol{k}_0}(t-t_0)\big]\sum_{s''} \tag{A10b}$$
$$\times \big(F_a\, L^{+,s';+,s'';\mu}_{2,1} L^{+,s'';+,s;\nu}_{1,0} \tag{A10c}$$
$$+ F_b\, L^{+,s';+,s'';\nu}_{2,1} L^{+,s'';+,s;\mu}_{1,0} \tag{A10d}$$
$$+ F_c\, L^{+,s';-,s'';\nu}_{2,1} L^{-,s'';+,s;\mu}_{1,0} \tag{A10e}$$
$$+ F_d\, L^{+,s';-,s'';\mu}_{2,1} L^{-,s'';+,s;\nu}_{1,0}\big), \tag{A10f}$$

with the prefactors

$$F_a = (\mathcal{E}_{\boldsymbol{k}_0} - \mathcal{E}_{\boldsymbol{k}_1} + k_l)^{-1}, \tag{A11a}$$
$$F_b = (\mathcal{E}_{\boldsymbol{k}_0} - \mathcal{E}_{\boldsymbol{k}_1} - k_l)^{-1}, \tag{A11b}$$
$$F_c = (\mathcal{E}_{\boldsymbol{k}_0} + \mathcal{E}_{\boldsymbol{k}_1} - k_l)^{-1}, \tag{A11c}$$
$$F_d = (\mathcal{E}_{\boldsymbol{k}_0} + \mathcal{E}_{\boldsymbol{k}_1} + k_l)^{-1}. \tag{A11d}$$

Note that the lower integration limit of the $t_1$ integral in Eq. (A7) is only contributing nonresonant terms, which are neglected in Eq. (A10).

## APPENDIX B: SECOND-ORDER TAYLOR EXPANSION OF THE SPIN-DEPENDENT ELECTRON SCATTERING MATRIX

For the terms in the last four lines in Eq. (A10), we define the expression

$$M^{s',s;\mu\nu} = m\sqrt{\frac{\mathcal{E}_{\boldsymbol{k}_2}}{m}}\sqrt{\frac{\mathcal{E}_{\boldsymbol{k}_0}}{m}}\sum_{s''} \tag{B1a}$$
$$\times \big(F_a\, L^{+,s';+,s'';\mu}_{2,1} L^{+,s'';+,s;\nu}_{1,0} \tag{B1b}$$
$$+ F_b\, L^{+,s';+,s'';\nu}_{2,1} L^{+,s'';+,s;\mu}_{1,0} \tag{B1c}$$
$$+ F_c\, L^{+,s';-,s'';\nu}_{2,1} L^{-,s'';+,s;\mu}_{1,0} \tag{B1d}$$
$$+ F_d\, L^{+,s';-,s'';\mu}_{2,1} L^{-,s'';+,s;\nu}_{1,0}\big), \tag{B1e}$$

such that Eq. (A10) can be written as

$$U_{2,0}^{+,s';+,s}(t,t_0) \approx -i\sqrt{\frac{m}{\mathcal{E}_{\boldsymbol{k}_2}}}\sqrt{\frac{m}{\mathcal{E}_{\boldsymbol{k}_0}}}\frac{\mathrm{e}^2 a'^{*}_{\mu} a_{\nu}}{4m} M^{s',s;\mu\nu} \times (t-t_0)\exp[-i\mathcal{E}_{\boldsymbol{k}_0}(t-t_0)]. \tag{B2}$$

The matrix elements $M^{s',s,\mu\nu}$ in (B1) are functions of the photon momentum $k_l$ and the two transverse photon momenta $k_2$ and $k_3$. For the following calculation, we introduce the scaled parameters

$$q_l = \frac{k_l}{m}, \quad q_2 = \frac{k_2}{m}, \quad q_3 = \frac{k_3}{m}, \tag{B3}$$

and

$$\tilde{q}_3 = \frac{k_3 - m}{m} = q_3 - 1. \tag{B4}$$

The Taylor expansion of $M^{s',s,\mu\nu}$ with respect to the three parameters (B3) is

$$M^{22} = \left(1 + \frac{\sqrt{2}-1}{2}q_l^2 - q_2^2\right)\mathbb{1} - \frac{i}{\sqrt{2}}\left[\left(\sqrt{2}-1\right) + \frac{3-2\sqrt{2}}{2}\tilde{q}_3\right]q_l\sigma_y - \frac{i}{\sqrt{2}}q_l q_2\sigma_z, \tag{B5a}$$

$$M^{23} = -q_2\mathbb{1} + \left[-\frac{i}{2}\sigma_x + \frac{i}{2}\tilde{q}_3\sigma_x + \frac{i}{2}q_2\sigma_y - \frac{i}{2}\sigma_z\right]q_l, \tag{B5b}$$

$$M^{32} = -q_2\mathbb{1} + \left[\frac{i}{2}\sigma_x - \frac{i}{2}\tilde{q}_3\sigma_x + \frac{i}{2}q_2\sigma_y - \frac{i}{2}\sigma_z\right]q_l, \tag{B5c}$$

$$M^{33} = \left[-\tilde{q}_3 + \frac{1}{2}\tilde{q}_3^2 + \frac{\sqrt{2}-1}{2}q_l^2 + \frac{q_2^2}{2}\right]\mathbb{1} - \frac{i}{\sqrt{2}}\left[-1 + \frac{3-2\sqrt{2}}{2}\tilde{q}_3\right]q_l\sigma_y + i\frac{\sqrt{2}-1}{\sqrt{2}}q_2 q_l\sigma_z. \tag{B5d}$$

Here, we have accounted for all contributions up to the quadratic order in the expansion parameters $q_l$, $q_2$, and $q_3$ and their mixed orders. Note that the Taylor expansion with respect to $q_l$ and $q_2$ is performed around their zero value, $k_l = 0$ and $k_2 = 0$, while the Taylor expansion with respect to $q_3$ is performed around the value $k_3 = m$, to get an approximate expression in the vicinity around the initial and final momenta $\tilde{\boldsymbol{p}}_i$ and $\tilde{\boldsymbol{p}}_f$ [as defined in Eqs. (5) and (7)], which the whole article is about. For this reason, we have rewritten the electron momentum $q_3$ into the shifted momentum $\tilde{q}_3$ in Eq. (B4), where the Taylor expansion around the value $k_3 = m$ corresponds to a Taylor expansion around $\tilde{q}_3 = 0$. We point out that the Taylor expanded matrix (B5) shows the same matrix entries as the matrix (5) in Ref. [71], with the addition that Eq. (B5) also shows the second-order terms of the Taylor expansion.

## APPENDIX C: PERTURBATIVE ELECTRON INTERACTION WITH A QUANTIZED PHOTON FIELD

### 1. Development of frame-fixed, quantized electron-photon Hamiltonian

We now want to perform a similar perturbative procedure as in Appendix A for a system where a single electron is interacting with a single photon and where particles are quantized in the context of a canonical quantization. Thus, we start by assuming the initial two-particle excitation,

$$\Psi_i = c_{\boldsymbol{p}_i}^{s\dagger} a_{\boldsymbol{k}}^{w\dagger}\,|0\rangle\,, \tag{C1}$$

where $c_{\boldsymbol{p}_i}^{s\dagger}$ is the electron creation operator with spin state $s$ and initial momentum $\boldsymbol{p}_i$, and $a_{\boldsymbol{k}}^{w\dagger}$ is the photon creation operator with polarization $w$ and momentum $\boldsymbol{k}$. The ket $|0\rangle$ is the quantum vacuum state with a zero number of electron and photon excitations. For the particle operators, we assume commutation relations $[\cdot,\cdot]$ for the photon particle operators and anticommutation $\{\cdot,\cdot\}$ for the electron particle and antiparticle operators,

$$\left[a_{\boldsymbol{k}}^{\lambda}, a_{\boldsymbol{k}'}^{\eta\dagger}\right] = \left\{c_{\boldsymbol{k}}^{\lambda}, c_{\boldsymbol{k}'}^{\eta\dagger}\right\} = \left\{d_{\boldsymbol{k}}^{\lambda}, d_{\boldsymbol{k}'}^{\eta\dagger}\right\} = \delta_{\boldsymbol{k},\boldsymbol{k}'}\delta_{\lambda,\eta}, \tag{C2a}$$

$$\left[a_{\boldsymbol{k}}^{r}, a_{\boldsymbol{k}'}^{t}\right] = \left\{c_{\boldsymbol{k}}^{s}, c_{\boldsymbol{k}'}^{s'}\right\} = \left\{d_{\boldsymbol{k}}^{s}, d_{\boldsymbol{k}'}^{s'}\right\} = 0\,. \tag{C2b}$$

We also assume that electron particle and antiparticle operators anticommute with each other and photon operators commute with electron particle and antiparticle operators,

$$\left\{c_{\boldsymbol{k}}^{s}, d_{\boldsymbol{k}'}^{s'}\right\} = \left\{c_{\boldsymbol{k}}^{s}, d_{\boldsymbol{k}'}^{s'\dagger}\right\} = 0, \tag{C2c}$$

$$\left[a_{\boldsymbol{k}}^{r}, c_{\boldsymbol{k}'}^{r}\right] = \left[a_{\boldsymbol{k}}^{r}, c_{\boldsymbol{k}'}^{r\dagger}\right] = 0, \tag{C2d}$$

$$\left[a_{\boldsymbol{k}}^{r}, d_{\boldsymbol{k}'}^{r}\right] = \left[a_{\boldsymbol{k}}^{r}, d_{\boldsymbol{k}'}^{r\dagger}\right] = 0. \tag{C2e}$$

Our aim is to find the perturbative time evolution under the action

$$\mathcal{L} = \bar{\Psi}\left(i\gamma_\mu\partial^\mu - m\right)\Psi - \tfrac{1}{4}F^{\mu\nu}F_{\mu\nu} - \mathrm{e}\bar{\Psi}\gamma_\mu\mathcal{A}^\mu\Psi, \tag{C3}$$

with Dirac field $\Psi$, photon field $\mathcal{A}^\mu$, and electromagnetic field tensor

$$F^{\mu\nu} = \partial^\mu\mathcal{A}^\nu - \partial^\nu\mathcal{A}^\mu, \tag{C4}$$

with the derivative

$$\partial^\mu = \frac{\partial}{\partial x_\mu}. \tag{C5}$$

The bar on top of $\Psi$ denotes the multiplication of its adjoint with $\gamma_0$, $\bar{\Psi} = \Psi^\dagger\gamma_0$. Regarding the QED Lagrangian (C3), we follow the conventions from standard quantum field theory; see Refs. [3,73,76,86–88] for an introduction.

The Lagrangian density in Eq. (C3) implies the free Hamiltonian for electrons and their antiparticles [89],

$$H_e = \sum_{\boldsymbol{k},s}\mathcal{E}_{\boldsymbol{k}}\left(c_{\boldsymbol{k}}^{s\dagger}c_{\boldsymbol{k}}^{s} + d_{\boldsymbol{k}}^{s\dagger}d_{\boldsymbol{k}}^{s}\right), \tag{C6}$$

as well as the free Hamiltonian for photons [89],

$$H_p = \sum_{\boldsymbol{k},r} k\, a^{r\dagger}_{\boldsymbol{k}} a^{r}_{\boldsymbol{k}}, \tag{C7}$$

where $k = |\boldsymbol{k}|$ is the dispersion of light in vacuum. Of particular interest for the time evolution is the interaction part of the Hamiltonian from the Hamiltonian density,

$$\mathcal{H} = \Pi\, \dot{\Psi} + \Pi^{\mu} \dot{\mathcal{A}}_{\mu} - \mathcal{L}, \tag{C8}$$

where $\Pi$ and $\Pi^{\mu}$ are the conjugated momenta of the Dirac field and the photon field, respectively. The interaction part of the Lagrangian density (C3) is

$$\mathcal{L}_{\rm int} = -\mathrm{e}\bar{\Psi}\gamma_{\mu}\mathcal{A}^{\mu}\Psi, \tag{C9}$$

implying the interaction part of the Hamiltonian density,

$$\mathcal{H}_{\rm int} = \mathrm{e}\bar{\Psi}\gamma_{\mu}\mathcal{A}^{\mu}\Psi. \tag{C10}$$

We denote the electron field operators $\Psi$, $\bar{\Psi}$ and photon field operator $\mathcal{A}_{\mu}$ by

$$\Psi(\boldsymbol{x},t) = \sum_{\boldsymbol{k},s} \left(c^{s}_{\boldsymbol{k}} u^{s}_{\boldsymbol{k}} e^{-ik\cdot x} + d^{s\dagger}_{\boldsymbol{k}} v^{s}_{\boldsymbol{k}} e^{ik\cdot x}\right), \tag{C11a}$$

$$\bar{\Psi}(\boldsymbol{x},t) = \sum_{\boldsymbol{k},s} \left(c^{s\dagger}_{\boldsymbol{k}} \bar{u}^{s}_{\boldsymbol{k}} e^{ik\cdot x} + d^{s}_{\boldsymbol{k}} \bar{v}^{s}_{\boldsymbol{k}} e^{-ik\cdot x}\right), \tag{C11b}$$

$$\mathcal{A}_{\mu}(\boldsymbol{x},t) = \sum_{\boldsymbol{k},r} \left(\epsilon^{(r)}_{\mu,\boldsymbol{k}} a^{r}_{\boldsymbol{k}} e^{-ik\cdot x} + \epsilon^{(r)*}_{\mu,\boldsymbol{k}} a^{r\dagger}_{\boldsymbol{k}} e^{ik\cdot x}\right), \tag{C11c}$$

where $u^{s}_{\boldsymbol{k}}$ and $v^{s}_{\boldsymbol{k}}$ are the bispinors (9) and $\epsilon^{(r)}_{\mu,\boldsymbol{k}}$ are the four ($r$ index) four-polarization ($\mu$ index) vectors of the photon field. Inserting the definitions (C11) in the interaction part of the Hamilton density (C10) yields the interaction Hamiltonian

$$H_{\rm int} = \mathrm{e}\int d^3x \bar{\Psi}\gamma_{\mu}\mathcal{A}^{\mu}\Psi = \mathrm{e}\sum_{\substack{\boldsymbol{k},\boldsymbol{k}'\\ s,s',r}} \tag{C12a}$$

$$\times\Big[\left(\bar{u}^{s}_{\boldsymbol{k}} \not{\epsilon}^{(r)}_{\boldsymbol{k}-\boldsymbol{k}'} u^{s'}_{\boldsymbol{k}'}\right) c^{s\dagger}_{\boldsymbol{k}} c^{s'}_{\boldsymbol{k}'} a^{r}_{\boldsymbol{k}-\boldsymbol{k}'} \tag{C12b}$$

$$+\left(\bar{u}^{s}_{\boldsymbol{k}} \not{\epsilon}^{(r)*}_{-\boldsymbol{k}+\boldsymbol{k}'} u^{s'}_{\boldsymbol{k}'}\right) c^{s\dagger}_{\boldsymbol{k}} c^{s'}_{\boldsymbol{k}'} a^{r\dagger}_{-\boldsymbol{k}+\boldsymbol{k}'} \tag{C12c}$$

$$+\left(\bar{v}^{s}_{-\boldsymbol{k}} \not{\epsilon}^{(r)}_{\boldsymbol{k}-\boldsymbol{k}'} u^{s'}_{\boldsymbol{k}'}\right) d^{s}_{-\boldsymbol{k}} c^{s'}_{\boldsymbol{k}'} a^{r}_{\boldsymbol{k}-\boldsymbol{k}'} \tag{C12d}$$

$$+\left(\bar{v}^{s}_{-\boldsymbol{k}} \not{\epsilon}^{(r)*}_{-\boldsymbol{k}+\boldsymbol{k}'} u^{s'}_{\boldsymbol{k}'}\right) d^{s}_{-\boldsymbol{k}} c^{s'}_{\boldsymbol{k}'} a^{r\dagger}_{-\boldsymbol{k}+\boldsymbol{k}'} \tag{C12e}$$

$$+\left(\bar{u}^{s}_{\boldsymbol{k}} \not{\epsilon}^{(r)}_{\boldsymbol{k}-\boldsymbol{k}'} v^{s'}_{-\boldsymbol{k}'}\right) c^{s\dagger}_{\boldsymbol{k}} d^{s'\dagger}_{-\boldsymbol{k}'} a^{r}_{\boldsymbol{k}-\boldsymbol{k}'} \tag{C12f}$$

$$+\left(\bar{u}^{s}_{\boldsymbol{k}} \not{\epsilon}^{(r)*}_{-\boldsymbol{k}+\boldsymbol{k}'} v^{s'}_{-\boldsymbol{k}'}\right) c^{s\dagger}_{\boldsymbol{k}} d^{s'\dagger}_{-\boldsymbol{k}'} a^{r\dagger}_{-\boldsymbol{k}+\boldsymbol{k}'} \tag{C12g}$$

$$+\left(\bar{v}^{s}_{-\boldsymbol{k}} \not{\epsilon}^{(r)}_{\boldsymbol{k}-\boldsymbol{k}'} v^{s'}_{-\boldsymbol{k}'}\right) d^{s}_{-\boldsymbol{k}} d^{s'\dagger}_{-\boldsymbol{k}'} a^{r}_{\boldsymbol{k}-\boldsymbol{k}'} \tag{C12h}$$

$$+\left(\bar{v}^{s}_{-\boldsymbol{k}} \not{\epsilon}^{(r)*}_{-\boldsymbol{k}+\boldsymbol{k}'} v^{s'}_{-\boldsymbol{k}'}\right) d^{s}_{-\boldsymbol{k}} d^{s'\dagger}_{-\boldsymbol{k}'} a^{r\dagger}_{-\boldsymbol{k}+\boldsymbol{k}'}\Big], \tag{C12i}$$

where we are using the Feynman slash notion $\not{\epsilon} = \epsilon_{\mu}\gamma^{\mu}$ for the abbreviation of the contraction of the Dirac gamma matrices with a four-vector. The obtained interaction Hamiltonian (C12), together with the free Hamiltonians (C6) and (C7), determine the time evolution of vacuum excitations in the Schrödinger picture by

$$i\dot{\Psi} = H\Psi, \tag{C13}$$

with

$$H = H_e + H_p + H_{\rm int}. \tag{C14}$$

### 2. Perturbative derivation with quantized Hamiltonian

From Eq. (C13), one can write the time evolution in the form of a Dyson series, whose second-order interaction term reads

$$\mathcal{U}(t,t_0) = \frac{1}{i^2}\int_{t_0}^{t} dt_2 \int_{t_0}^{t_2} dt_1 \times \mathcal{U}_0(t,t_2) H_{\rm int} \mathcal{U}_0(t_2,t_1) H_{\rm int} \mathcal{U}_0(t_1,t_0), \tag{C15}$$

which is formally similar to the second-order perturbation of the single-particle description (A4). Here, $\mathcal{U}_0(t,t_0)$ is the free propagation

$$\mathcal{U}_0(t,t_0) = \exp[-i(H_e + H_p)(t-t_0)] \tag{C16}$$

of electrons, their antiparticles, and photons. The first-order contributions of the Dyson series are not considered since they do not contain resonant terms due to energy and momentum conservation. For the initial state $\Psi_i$ in Eq. (C1), we obtain, from Eq. (C16),

$$\mathcal{U}_0(t_1,t_0) = \exp[-i(\mathcal{E}_{\boldsymbol{p}_i} + k)(t_1 - t_0)] \tag{C17}$$

for the time interval $[t_0,t_1]$ of the first free quantum state propagation in the second-order perturbation (C15). Note that while Eq. (C16) is an operator equation, the expressions in Eq. (C17) and also Eqs. (C20) and (C24), shown below, are expressions where the operators have been acting at the operators of the quantum states and turned into ordinary complex numbers by the eigenvalue operations of the operators.

The first action of $H_{\rm int}$ on $\Psi_i$ results in the intermediate states,

$$\Psi_a = c^{s''\dagger}_{\boldsymbol{p}_i+\boldsymbol{k}} |0\rangle, \tag{C18a}$$

$$\Psi_b = c^{s''\dagger}_{\boldsymbol{p}_i-\boldsymbol{k}'} a^{w\dagger}_{\boldsymbol{k}} a^{r\dagger}_{\boldsymbol{k}'} |0\rangle, \tag{C18b}$$

$$\Psi_c = c^{s\dagger}_{\boldsymbol{p}_i} c^{s'\dagger}_{\boldsymbol{p}_f} d^{s''\dagger}_{-\boldsymbol{p}_i+\boldsymbol{k}'} |0\rangle, \tag{C18c}$$

$$\Psi_d = c^{s\dagger}_{\boldsymbol{p}_i} c^{s'\dagger}_{\boldsymbol{p}_f} d^{s''\dagger}_{-\boldsymbol{p}_i-\boldsymbol{k}} a^{w\dagger}_{\boldsymbol{k}} a^{r\dagger}_{\boldsymbol{k}'} |0\rangle, \tag{C18d}$$

where the interaction term

$$\left(\bar{u}^{s''}_{\boldsymbol{p}_i+\boldsymbol{k}} \not{\epsilon}^{(w)}_{\boldsymbol{k}} u^{s}_{\boldsymbol{p}_i}\right) c^{s''\dagger}_{\boldsymbol{p}_i+\boldsymbol{k}} c^{s}_{\boldsymbol{p}_i} a^{w}_{\boldsymbol{k}} \quad \text{maps to } \Psi_a, \tag{C19a}$$

$$\left(\bar{u}^{s''}_{\boldsymbol{p}_i-\boldsymbol{k}'} \not{\epsilon}^{(r)*}_{\boldsymbol{k}'} u^{s}_{\boldsymbol{p}_i}\right) c^{s''\dagger}_{\boldsymbol{p}_i-\boldsymbol{k}'} c^{s}_{\boldsymbol{p}_i} a^{r\dagger}_{\boldsymbol{k}'} \quad \text{maps to } \Psi_b, \tag{C19b}$$

$$\left(\bar{u}^{s'}_{\boldsymbol{p}_f} \not{\epsilon}^{(w)}_{\boldsymbol{k}} v^{s''}_{-\boldsymbol{p}_i+\boldsymbol{k}'}\right) c^{s'\dagger}_{\boldsymbol{p}_f} d^{s''\dagger}_{-\boldsymbol{p}_i+\boldsymbol{k}'} a^{w}_{\boldsymbol{k}} \quad \text{maps to } \Psi_c, \tag{C19c}$$

$$\left(\bar{u}^{s'}_{\boldsymbol{p}_f} \not{\epsilon}^{(r)*}_{\boldsymbol{k}'} v^{s''}_{-\boldsymbol{p}_i-\boldsymbol{k}}\right) c^{s'\dagger}_{\boldsymbol{p}_f} d^{s''\dagger}_{-\boldsymbol{p}_i-\boldsymbol{k}} a^{r\dagger}_{\boldsymbol{k}'} \quad \text{maps to } \Psi_d, \tag{C19d}$$

as illustrated in Fig. 1. In correspondence, for the time interval $[t_1,t_2]$ of the second free propagation in (C15), one obtains the free propagation

$$\mathcal{U}_0(t_2,t_1) = \exp[-i(\mathcal{E}_{\boldsymbol{p}_i+\boldsymbol{k}})(t_2-t_1)],$$

$$\mathcal{U}_0(t_2,t_1) = \exp[-i(\mathcal{E}_{\boldsymbol{p}_i-\boldsymbol{k}'} + k + k')(t_2-t_1)],$$

$$\mathcal{U}_0(t_2,t_1) = \exp[-i(\mathcal{E}_{\boldsymbol{p}_i} + \mathcal{E}_{\boldsymbol{p}_f} + \mathcal{E}_{-\boldsymbol{p}_i+\boldsymbol{k}'})(t_2-t_1)],$$
$$\mathcal{U}_0(t_2,t_1) = \exp[-i(\mathcal{E}_{\boldsymbol{p}_i} + \mathcal{E}_{\boldsymbol{p}_f} + \mathcal{E}_{-\boldsymbol{p}_i-\boldsymbol{k}} + k + k')(t_2-t_1)], \tag{C20}$$

for $\Psi_a$, $\Psi_b$, $\Psi_c$, and $\Psi_d$, respectively. For the following second interaction $H_{\rm int}$ in Eq. (C15), only terms which fulfill energy conservation are relevant, as all other contributions will oscillate in off-resonant Rabi cycles of low amplitude. Particle excitations different than

$$\Psi_f = c^{s'\dagger}_{\boldsymbol{p}_f} a^{r\dagger}_{\boldsymbol{k}'} |0\rangle \tag{C21}$$

are therefore not possible for asymptotically long times, with the final electron momentum $\boldsymbol{p}_f = \boldsymbol{p}_i + \boldsymbol{k} - \boldsymbol{k}'$ and photon momentum $\boldsymbol{k}'$. The corresponding energy conservation relation of the constituting particles displays as

$$\mathcal{E}_{\boldsymbol{p}_i} + k = \mathcal{E}_{\boldsymbol{p}_f} + k'. \tag{C22}$$

According to the above considerations, the only contributions in the interaction Hamiltonian (C12) that map back to the final state $\Psi_f$ are

$$\big(\bar{u}^{s'}_{\boldsymbol{p}_f} \not{\epsilon}^{(r)*}_{\boldsymbol{k}'} u^{s''}_{\boldsymbol{p}_i+\boldsymbol{k}}\big) c^{s'\dagger}_{\boldsymbol{p}_f} c^{s''}_{\boldsymbol{p}_i+\boldsymbol{k}} a^{r\dagger}_{\boldsymbol{k}'} \quad \text{from } \Psi_a, \tag{C23a}$$
$$\big(\bar{u}^{s'}_{\boldsymbol{p}_f} \not{\epsilon}^{(w)}_{\boldsymbol{k}} u^{s''}_{\boldsymbol{p}_i-\boldsymbol{k}'}\big) c^{s'\dagger}_{\boldsymbol{p}_f} c^{s''}_{\boldsymbol{p}_i-\boldsymbol{k}'} a^{w}_{\boldsymbol{k}} \quad \text{from } \Psi_b, \tag{C23b}$$
$$\big(\bar{v}^{s''}_{-\boldsymbol{p}_i+\boldsymbol{k}'} \not{\epsilon}^{(r)*}_{\boldsymbol{k}'} u^{s}_{\boldsymbol{p}_i}\big) d^{s''}_{-\boldsymbol{p}_i+\boldsymbol{k}'} c^{s}_{\boldsymbol{p}_i} a^{r\dagger}_{\boldsymbol{k}'} \quad \text{from } \Psi_c, \tag{C23c}$$
$$\big(\bar{v}^{s''}_{-\boldsymbol{p}_i-\boldsymbol{k}} \not{\epsilon}^{(w)}_{\boldsymbol{k}} u^{s}_{\boldsymbol{p}_i}\big) d^{s''}_{-\boldsymbol{p}_i-\boldsymbol{k}} c^{s}_{\boldsymbol{p}_i} a^{w}_{\boldsymbol{k}} \quad \text{from } \Psi_d. \tag{C23d}$$

The free propagation (C16) of the final state $\Psi_f$ evaluates to

$$\mathcal{U}_0(t,t_2) = \exp[-i(\mathcal{E}_{\boldsymbol{p}_f} + k')(t-t_2)] \tag{C24a}$$
$$= \exp[-i(\mathcal{E}_{\boldsymbol{p}_i} + k)(t-t_2)], \tag{C24b}$$

and its phase oscillates with the same frequency as the free propagation of $\Psi_i$ in Eq. (C17) due to the energy conservation relation (C22). Consequently, the oscillations of the perturbative contribution of the propagator (C15) with respect to the integration variables $t_1$ and $t_2$ oscillate in the exponential with the factor

$$-i(\mathcal{E}_{\boldsymbol{p}_i+\boldsymbol{k}} - \mathcal{E}_{\boldsymbol{p}_i} - k)(t_2-t_1), \tag{C25a}$$
$$-i(\mathcal{E}_{\boldsymbol{p}_i-\boldsymbol{k}'} - \mathcal{E}_{\boldsymbol{p}_i} + k')(t_2-t_1), \tag{C25b}$$
$$-i(\mathcal{E}_{-\boldsymbol{p}_i+\boldsymbol{k}'} + \mathcal{E}_{\boldsymbol{p}_i} - k')(t_2-t_1), \tag{C25c}$$
$$-i(\mathcal{E}_{-\boldsymbol{p}_i-\boldsymbol{k}} + \mathcal{E}_{\boldsymbol{p}_i} + k)(t_2-t_1), \tag{C25d}$$

for $\Psi_a$, $\Psi_b$, $\Psi_c$, and $\Psi_d$, respectively. Note that Eq. (C22) has been substituted to arrive at (C25).

For the upper integration limit of the integral with respect to $t_1$ in Eq. (C15), the phase terms (C25) are canceling to zero, such that the integration with respect to $t_2$ will be independent of $t_2$, resulting in a solution which is growing linear in time, similar to the perturbative single-particle calculation in Appendix A. In accordance, the integration with respect to $t_1$ yields the prefactors

$$\mathcal{F}_a = (\mathcal{E}_{\boldsymbol{p}_i} - \mathcal{E}_{\boldsymbol{p}_i+\boldsymbol{k}} + k)^{-1}, \tag{C26a}$$
$$\mathcal{F}_b = (\mathcal{E}_{\boldsymbol{p}_i} - \mathcal{E}_{\boldsymbol{p}_i-\boldsymbol{k}'} - k')^{-1}, \tag{C26b}$$
$$\mathcal{F}_c = (\mathcal{E}_{\boldsymbol{p}_i} + \mathcal{E}_{\boldsymbol{p}_i-\boldsymbol{k}'} - k')^{-1}, \tag{C26c}$$
$$\mathcal{F}_d = (\mathcal{E}_{\boldsymbol{p}_i} + \mathcal{E}_{\boldsymbol{p}_i+\boldsymbol{k}} + k)^{-1}, \tag{C26d}$$

in Eq. (C15), which are the analogue to the prefactors (A11). Note that we accounted for an additional minus sign for Eqs. (C26c) and (C26d) due to the commutation relations (C2) of the additional virtual electron-positron pair and we multiplied all terms with another factor $i^{-1}$ for ease of notion. We also made use of $\mathcal{E}_{\boldsymbol{p}} = \mathcal{E}_{-\boldsymbol{p}}$ for the determination of the factors (C26) from (C25).

Taking the prefactors (C26), together with the corresponding interaction matrix elements in (C19) and (C23), and substituting them into the propagator (C15) results in the expression

$$\begin{aligned}\mathcal{U}^{s',s;r,w}(t,t_0) = -i\mathrm{e}^2(t-t_0)\exp[-i(\mathcal{E}_{\boldsymbol{p}_i}+k)(t-t_0)] \\ \times \sum_{s''} \big[\mathcal{F}_a \big(\bar{u}^{s'}_{\boldsymbol{p}_f} \not{\epsilon}^{(r)*}_{\boldsymbol{k}'} u^{s''}_{\boldsymbol{p}_i+\boldsymbol{k}}\big)\big(\bar{u}^{s''}_{\boldsymbol{p}_i+\boldsymbol{k}} \not{\epsilon}^{(w)}_{\boldsymbol{k}} u^{s}_{\boldsymbol{p}_i}\big) \\ + \mathcal{F}_b \big(\bar{u}^{s'}_{\boldsymbol{p}_f} \not{\epsilon}^{(w)}_{\boldsymbol{k}} u^{s''}_{\boldsymbol{p}_i-\boldsymbol{k}'}\big)\big(\bar{u}^{s''}_{\boldsymbol{p}_i-\boldsymbol{k}'} \not{\epsilon}^{(r)*}_{\boldsymbol{k}'} u^{s}_{\boldsymbol{p}_i}\big) \\ + \mathcal{F}_c \big(\bar{u}^{s'}_{\boldsymbol{p}_f} \not{\epsilon}^{(w)}_{\boldsymbol{k}} v^{s''}_{-\boldsymbol{p}_i+\boldsymbol{k}'}\big)\big(\bar{v}^{s''}_{-\boldsymbol{p}_i+\boldsymbol{k}'} \not{\epsilon}^{(r)*}_{\boldsymbol{k}'} u^{s}_{\boldsymbol{p}_i}\big) \\ + \mathcal{F}_d \big(\bar{u}^{s'}_{\boldsymbol{p}_f} \not{\epsilon}^{(r)*}_{\boldsymbol{k}'} v^{s''}_{-\boldsymbol{p}_i-\boldsymbol{k}}\big)\big(\bar{v}^{s''}_{-\boldsymbol{p}_i-\boldsymbol{k}} \not{\epsilon}^{(w)}_{\boldsymbol{k}} u^{s}_{\boldsymbol{p}_i}\big)\big].\end{aligned} \tag{C27}$$

In technical terms, the propagator (C27) should be understood in the following way: The operator $\mathcal{U}(t,t_0)$ in Eq. (C15) is applied at the initial quantum state $c^{s\dagger}_{\boldsymbol{p}_i} a^{w\dagger}_{\boldsymbol{k}} |0\rangle$ in Eq. (C1) and the propagation matrix (C27) determines the amplitude of the final states $c^{s'\dagger}_{\boldsymbol{p}_f} a^{r\dagger}_{\boldsymbol{k}'} |0\rangle$ of Eq. (C21). These final states are the only relevant resonant states, which are seen as nonvanishing contributions after long times $t$. In this context, we conclude the approximate relation

$$\mathcal{U}(t,t_0)\, c^{s\dagger}_{\boldsymbol{p}_i} a^{w\dagger}_{\boldsymbol{k}} |0\rangle \approx \sum_{s',r} \mathcal{U}^{s',s;r,w}(t,t_0)\, c^{s'\dagger}_{\boldsymbol{p}_f} a^{r\dagger}_{\boldsymbol{k}'} |0\rangle \tag{C28}$$

for a perturbative electron-photon interaction. The spin and polarization properties of $\Psi_f$ are determined by matrix entries as in Eq. (B5) for the scattering scenario, as described in Secs. II and III. Correspondingly, we find

$$\mathcal{U}(t,t_0)\, c^{\searrow\dagger}_{\tilde{\boldsymbol{p}}_i} a^{3\dagger}_{\boldsymbol{k}_l} |0\rangle \approx f(t,t_0)\, c^{\nwarrow\dagger}_{\tilde{\boldsymbol{p}}_f} a^{\mathrm{L}\dagger}_{-\boldsymbol{k}_l} |0\rangle\,, \tag{C29a}$$
$$\mathcal{U}(t,t_0)\, c^{\nwarrow\dagger}_{\tilde{\boldsymbol{p}}_i} a^{3\dagger}_{\boldsymbol{k}_l} |0\rangle \approx f(t,t_0)\, c^{\searrow\dagger}_{\tilde{\boldsymbol{p}}_f} a^{\mathrm{R}\dagger}_{-\boldsymbol{k}_l} |0\rangle\,, \tag{C29b}$$

with the time-dependent prefactor

$$f(t,t_0) = \mathrm{e}^2(t-t_0)\exp[-i(\mathcal{E}_{\boldsymbol{p}_i}+k)(t-t_0)]. \tag{C30}$$

Here, the tilted spin electron creation and annihilation operators can be expressed in terms of the spin-up and spin-down electron creation operators $c^{\uparrow\dagger}_{\boldsymbol{p}}$ and $c^{\downarrow\dagger}_{\boldsymbol{p}}$ and the spin states $s^{\searrow}$

and $s^{\nwarrow}$ of Eq. (6) and Eq. (16) by

$$c_{\boldsymbol{p}}^{\searrow\dagger} = s_1^{\searrow} c_{\boldsymbol{p}}^{\uparrow\dagger} + s_2^{\searrow} c_{\boldsymbol{p}}^{\downarrow\dagger}, \tag{C31a}$$

$$c_{\boldsymbol{p}}^{\nwarrow\dagger} = s_1^{\nwarrow} c_{\boldsymbol{p}}^{\uparrow\dagger} + s_2^{\nwarrow} c_{\boldsymbol{p}}^{\downarrow\dagger}. \tag{C31b}$$

Also, the left- and right-handed photon creation operators in (C29) are defined by

$$a_{\boldsymbol{k}_l}^{L\dagger} = a_{\boldsymbol{k}_l}^{2\dagger} - i a_{\boldsymbol{k}_l}^{3\dagger}, \tag{C32a}$$

$$a_{\boldsymbol{k}_l}^{R\dagger} = a_{\boldsymbol{k}_l}^{2\dagger} + i a_{\boldsymbol{k}_l}^{3\dagger}, \tag{C32b}$$

$$a_{-\boldsymbol{k}_l}^{L\dagger} = a_{-\boldsymbol{k}_l}^{2\dagger} + i a_{-\boldsymbol{k}_l}^{3\dagger}, \tag{C32c}$$

$$a_{-\boldsymbol{k}_l}^{R\dagger} = a_{-\boldsymbol{k}_l}^{2\dagger} - i a_{-\boldsymbol{k}_l}^{3\dagger}. \tag{C32d}$$

We point out that Eq. (C29) is the corresponding expression to Eq. (19) in Ref. [71]. However, in contrast to Ref. [71], the definitions (C32) contain consistent helicities of the photons which are propagating in the $x$ or $-x$ direction, in contrast to the left and right circular polarization introduced in Ref. [71]. Also, note that Ref. [71] is not accounting for the complex conjugation of the outgoing photon polarization in the Compton scattering formula (C38) (see, for example, [86]). In this work, both issues are accounted for.

### 3. Identification with Compton scattering formula from quantum field theory

The photon-polarization-dependent electron spin-coupling matrix in Eq. (C27) consists of the components

$$\sum_{s''} \mathcal{F}_a \big(\bar{u}_{\boldsymbol{p}_f}^{s'} \not{\epsilon}_{\boldsymbol{k}'}^{(r)*} u_{\boldsymbol{p}_i+\boldsymbol{k}}^{s''}\big)\big(\bar{u}_{\boldsymbol{p}_i+\boldsymbol{k}}^{s''} \not{\epsilon}_{\boldsymbol{k}}^{(w)} u_{\boldsymbol{p}_i}^{s}\big), \tag{C33a}$$

$$\sum_{s''} \mathcal{F}_b \big(\bar{u}_{\boldsymbol{p}_f}^{s'} \not{\epsilon}_{\boldsymbol{k}}^{(w)} u_{\boldsymbol{p}_i-\boldsymbol{k}'}^{s''}\big)\big(\bar{u}_{\boldsymbol{p}_i-\boldsymbol{k}'}^{s''} \not{\epsilon}_{\boldsymbol{k}'}^{(r)*} u_{\boldsymbol{p}_i}^{s}\big), \tag{C33b}$$

$$\sum_{s''} \mathcal{F}_c \big(\bar{u}_{\boldsymbol{p}_f}^{s'} \not{\epsilon}_{\boldsymbol{k}}^{(w)} v_{-\boldsymbol{p}_i+\boldsymbol{k}'}^{s''}\big)\big(\bar{v}_{-\boldsymbol{p}_i+\boldsymbol{k}'}^{s''} \not{\epsilon}_{\boldsymbol{k}'}^{(r)*} u_{\boldsymbol{p}_i}^{s}\big), \tag{C33c}$$

$$\sum_{s''} \mathcal{F}_d \big(\bar{u}_{\boldsymbol{p}_f}^{s'} \not{\epsilon}_{\boldsymbol{k}'}^{(r)*} v_{-\boldsymbol{p}_i-\boldsymbol{k}}^{s''}\big)\big(\bar{v}_{-\boldsymbol{p}_i-\boldsymbol{k}}^{s''} \not{\epsilon}_{\boldsymbol{k}}^{(w)} u_{\boldsymbol{p}_i}^{s}\big), \tag{C33d}$$

where each line corresponds to the intermediate quantum states (C18) and the corresponding spin- and polarization-dependent matrix elements as well as prefactors have been denoted in Eqs. (C19), (C23), and (C26), respectively. These expressions can be further simplified to appear as final $S$-matrix expressions in quantum field theory. First, we can substitute the identities

$$\sum_s u_{\boldsymbol{p}}^s \bar{u}_{\boldsymbol{p}}^s = \frac{\not{p} + m}{2\mathcal{E}_{\boldsymbol{p}}}, \tag{C34a}$$

$$\sum_s v_{\boldsymbol{p}}^s \bar{v}_{\boldsymbol{p}}^s = \frac{\not{p} - m}{2\mathcal{E}_{\boldsymbol{p}}}, \tag{C34b}$$

into the expressions (C33), resulting in

$$(\mathcal{F}_a - \mathcal{F}_d)\bar{u}_{\boldsymbol{p}_f}^{s'} \not{\epsilon}_{\boldsymbol{k}'}^{(r)*} \frac{\not{p}_i + \not{k} + m}{2\mathcal{E}_{\boldsymbol{p}_i+\boldsymbol{k}}} \not{\epsilon}_{\boldsymbol{k}}^{(w)} u_{\boldsymbol{p}_i}^{s}, \tag{C35a}$$

$$(\mathcal{F}_b - \mathcal{F}_c)\bar{u}_{\boldsymbol{p}_f}^{s'} \not{\epsilon}_{\boldsymbol{k}}^{(w)} \frac{\not{p}_i - \not{k}' + m}{2\mathcal{E}_{\boldsymbol{p}_i-\boldsymbol{k}'}} \not{\epsilon}_{\boldsymbol{k}'}^{(r)*} u_{\boldsymbol{p}_i}^{s}. \tag{C35b}$$

Equations (C33a) and (C33d), as well as Eqs. (C33b) and (C33c), are summed up into Eq. (C35a) and Eq. (C35b), respectively. In Eq. (C35a), we can simplify

$$\frac{\mathcal{F}_a - \mathcal{F}_d}{2\mathcal{E}_{\boldsymbol{p}_i+\boldsymbol{k}}} = \frac{1}{(\mathcal{E}_{\boldsymbol{p}_i} + k)^2 - (\mathcal{E}_{\boldsymbol{p}_i+\boldsymbol{k}})^2} = \frac{1}{2p_i \cdot k}, \tag{C36}$$

and, similarly, in Eq. (C35b), we can simplify

$$\frac{\mathcal{F}_b - \mathcal{F}_c}{2\mathcal{E}_{\boldsymbol{p}_i-\boldsymbol{k}'}} = \frac{1}{(\mathcal{E}_{\boldsymbol{p}_i} - k')^2 - (\mathcal{E}_{\boldsymbol{p}_i-\boldsymbol{k}'})^2} = -\frac{1}{2p_i \cdot k'}. \tag{C37}$$

Also summing up Eqs. (C35a) and (C35b) finally results in the Compton scattering formula,

$$\bar{u}_{\boldsymbol{p}_f}^{s'} \left( \not{\epsilon}_{\boldsymbol{k}'}^{(r)*} \frac{\not{p}_i + \not{k} + m}{2p_i \cdot k} \not{\epsilon}_{\boldsymbol{k}}^{(w)} - \not{\epsilon}_{\boldsymbol{k}}^{(w)} \frac{\not{p}_i - \not{k}' + m}{2p_i \cdot k'} \not{\epsilon}_{\boldsymbol{k}'}^{(r)*} \right) u_{\boldsymbol{p}_i}^{s}. \tag{C38}$$

Note that Eq. (C38) is a rewritten version of Eq. (C33), which in turn can be associated with the perturbative solution in Eqs. (A10c) until (A10f) for spin-dependent electron diffraction. A difference between both expressions is that (A10) is constructed from a standing light wave situation with $\boldsymbol{k} = -\boldsymbol{k}'$, whereas in the expressions in (C33), the wave vectors $\boldsymbol{k}$ and $\boldsymbol{k}'$ could be chosen independently. Also, we have used the abbreviation $L_{n,n'}^{\gamma,s;\gamma',s';\mu}$ for abbreviating the matrix elements (A3) in (A10). We point out that our calculations explicitly show that the spin- and polarization-dependent interaction of an electron with a photon in the process of Compton scattering (C38) matches the perturbative description of spin-dependent diffraction dynamics of an electron in an external potential of two plane waves (A10). In other words, the polarization properties in Compton scattering and in electron diffraction of the Kapitza-Dirac effect are of identical form; only the interpretation of the associated process is different, depending on the scenario under consideration (i.e., whether the scenario is Compton scattering or electron diffraction).

Further details about the calculation in this section can be found in the literature under the name "old-fashioned perturbation theory;" see, for example, [3,76].

## APPENDIX D: SPIN PROJECTION OF PROPAGATOR

Assume that $U^{+,+}$ is a complex $2 \times 2$ matrix, which represents the propagation of a two-component spinor. Then the following matrix elements can be written as

$$\langle s^{\searrow} | U_{a,b}^{+;+} | s^{\searrow} \rangle = \frac{1}{\sqrt{8}} \big[ (1-\sqrt{2}) U_{a,b}^{+,\uparrow;+,\uparrow} - U_{a,b}^{+,\uparrow;+,\downarrow} - U_{a,b}^{+,\downarrow;+,\uparrow} - (1+\sqrt{2}) U_{a,b}^{+,\downarrow;+,\downarrow} \big], \tag{D1a}$$

$$\langle s^{\searrow} | U_{a,b}^{+;+} | s^{\nwarrow} \rangle = \frac{1}{\sqrt{8}} \big[ -U_{a,b}^{+,\uparrow;+,\uparrow} - (1-\sqrt{2}) U_{a,b}^{+,\uparrow;+,\downarrow} - (1+\sqrt{2}) U_{a,b}^{+,\downarrow;+,\uparrow} + U_{a,b}^{+,\downarrow;+,\downarrow} \big], \tag{D1b}$$

$$\langle s^{\nwarrow}|\,U_{a,b}^{+;+}\,|\,s^{\searrow}\rangle = \frac{1}{\sqrt{8}}\big[-U_{a,b}^{+,\uparrow;+,\uparrow} - (1+\sqrt{2})U_{a,b}^{+,\uparrow;+,\downarrow} - (1-\sqrt{2})U_{a,b}^{+,\downarrow;+,\uparrow} + U_{a,b}^{+,\downarrow;+,\downarrow}\big], \tag{D1c}$$

$$\langle s^{\nwarrow}|\,U_{a,b}^{+;+}\,|\,s^{\nwarrow}\rangle = \frac{1}{\sqrt{8}}\big[-(1+\sqrt{2})U_{a,b}^{+,\uparrow;+,\uparrow} + U_{a,b}^{+,\uparrow;+,\downarrow} + U_{a,b}^{+,\downarrow;+,\uparrow} + (1-\sqrt{2})U_{a,b}^{+,\downarrow;+,\downarrow}\big]. \tag{D1d}$$


[1] More specifically, the spin is an intrinsic angular momentum of every elementary particle, where different elementary particles have different values of total spin angular momentum. In the exceptional case of the Higgs boson, the total spin angular momentum is 0, being therefore a spinless scalar particle. The other known elementary particles have a total spin angular momentum larger than 0.

[2] E. Wigner, On unitary representations of the inhomogeneous Lorentz group, Ann. Math. **40**, 149 (1939).

[3] S. Weinberg, *The Quantum Theory of Fields*, Vol. I (Cambridge University Press, Cambridge, 1995).

[4] M. Morrison, Spin: All is not what it seems, Stud. Hist. Philos. Sci. Part B: Stud. Hist. Philos. Modern Phys. **38**, 529 (2007).

[5] W. Gerlach and O. Stern, The experimental proof of the direction quantization in a magnetic field, Z. Phys. **9**, 349 (1922).

[6] W. Gerlach and O. Stern, The magnetic moment of the silver atom, Z. Phys. **9**, 353 (1922).

[7] W. Gerlach and O. Stern, The experimental proof of the magnetic moment of the silver atom, Z. Phys. **8**, 110 (1922).

[8] J. Kirschner, R. Feder, and J. F. Wendelken, Electron Spin Polarization In Energy- And Angle-Resolved Photoemission From W(001): Experiment And Theory, Phys. Rev. Lett. **47**, 614 (1981).

[9] T. Maruyama, E. L. Garwin, R. Prepost, G. H. Zapalac, J. S. Smith, and J. D. Walker, Observation Of Strain-Enhanced Electron-Spin Polarization In Photoemission From InGaAs, Phys. Rev. Lett. **66**, 2376 (1991).

[10] F. Meier, H. Dil, J. Lobo-Checa, L. Patthey, and J. Osterwalder, Quantitative vectorial spin analysis in angle-resolved photoemission: Bi/Ag(111) and Pb/Ag(111), Phys. Rev. B **77**, 165431 (2008).

[11] K. He, Y. Takeichi, M. Ogawa, T. Okuda, P. Moras, D. Topwal, A. Harasawa, T. Hirahara, C. Carbone, A. Kakizaki, and I. Matsuda, Direct Spectroscopic Evidence of Spin-Dependent Hybridization Between Rashba-Split Surface States And Quantum-Well States, Phys. Rev. Lett. **104**, 156805 (2010).

[12] H. Bentmann, T. Kuzumaki, G. Bihlmayer, S. Blügel, E. V. Chulkov, F. Reinert, and K. Sakamoto, Spin orientation and sign of the Rashba splitting in Bi/Cu(111), Phys. Rev. B **84**, 115426 (2011).

[13] D. Kutnyakhov, H. J. Elmers, G. Schönhense, C. Tusche, S. Borek, J. Braun, J. Minár, and H. Ebert, Specular reflection of spin-polarized electrons from the W(001) spin-filter crystal in a large range of scattering energies and angles, Phys. Rev. B **91**, 014416 (2015).

[14] H. J. Elmers, R. Wallauer, M. Liebmann, J. Kellner, M. Morgenstern, R. N. Wang, J. E. Boschker, R. Calarco, J. Sánchez-Barriga, O. Rader, D. Kutnyakhov, S. V. Chernov, K. Medjanik, C. Tusche, M. Ellguth, H. Volfova, S. Borek, J. Braun, J. Minár, H. Ebert, and G. Schönhense, Spin mapping of surface and bulk Rashba states in ferroelectric $\alpha$-GeTe(111) films, Phys. Rev. B **94**, 201403(R) (2016).

[15] R. Noguchi, K. Kuroda, K. Yaji, K. Kobayashi, M. Sakano, A. Harasawa, T. Kondo, F. Komori, and S. Shin, Direct mapping of spin and orbital entangled wave functions under interband spin-orbit coupling of giant Rashba spin-split surface states, Phys. Rev. B **95**, 041111(R) (2017).

[16] W. X. Tang, D. M. Paganin, and W. Wan, Proposal for electron quantum spin talbot effect, Phys. Rev. B **85**, 064418 (2012).

[17] W. Pauli, The quantum theories of magnetism. The magnetic electron, Proceedings of the Sixth Solvay Conference on Physics and Magnetism, in *Collected Scientific Papers*, Vol. 2, edited by R. Kronig and V. F. Weisskopf (Wiley, New York, 1964), pp. 544–552.

[18] N. F. Mott and H. S. W. Massey, *The Theory of Atomic Collisions*, 3rd ed. (The International Series of Monographs on Physics Oxford University Press, Oxford, United Kingdom, 1965).

[19] J. Kessler, *Polarized Electrons* (Springer, New York, 1976).

[20] H. Batelaan, T. J. Gay, and J. J. Schwendiman, Stern-Gerlach Effect For Electron Beams, Phys. Rev. Lett. **79**, 4517 (1997).

[21] G. H. Rutherford and R. Grobe, Comment on "Stern-Gerlach Effect For Electron Beams", Phys. Rev. Lett. **81**, 4772 (1998).

[22] G. A. Gallup, H. Batelaan, and T. J. Gay, Quantum-Mechanical Analysis Of A Longitudinal Stern-Gerlach Effect, Phys. Rev. Lett. **86**, 4508 (2001).

[23] H. Dehmelt, New continuous Stern-Gerlach effect and a hint of "the" elementary particle, Z. Phys. D Atoms Mol. Clusters **10**, 127 (1988).

[24] H. Dehmelt, Experiments on the structure of an individual elementary particle, Science **247**, 539 (1990).

[25] P. L. Kapitza and P. A. M. Dirac, The reflection of electrons from standing light waves, Math. Proc. Cambridge Philos. Soc. **29**, 297 (1933).

[26] M. Federov and J. McIver, Multiphoton stimulated Compton scattering, Opt. Commun. **32**, 179 (1980).

[27] R. Gush and H. P. Gush, Electron scattering from a standing light wave, Phys. Rev. D **3**, 1712 (1971).

[28] M. A. Efremov and M. V. Fedorov, Classical and quantum versions of the Kapitza-Dirac effect, J. Expt. Theor. Phys. **89**, 460 (1999).

[29] M. A. Efremov and M. V. Fedorov, Wavepacket theory of the Kapitza-Dirac effect, J. Phys. B: At., Mol. Opt. Phys. **33**, 4535 (2000).

[30] O. Smirnova, D. L. Freimund, H. Batelaan, and M. Ivanov, Kapitza-Dirac Diffraction Without Standing Waves: Diffraction Without A Grating? Phys. Rev. Lett. **92**, 223601 (2004).

[31] X. Li, J. Zhang, Z. Xu, P. Fu, D.-S. Guo, and R. R. Freeman, Theory Of The Kapitza-Dirac Diffraction Effect, Phys. Rev. Lett. **92**, 233603 (2004).

[32] P. L. Gould, G. A. Ruff, and D. E. Pritchard, Diffraction Of Atoms By Light: The Near-Resonant Kapitza-Dirac Effect, Phys. Rev. Lett. **56**, 827 (1986).
[33] P. J. Martin, B. G. Oldaker, A. H. Miklich, and D. E. Pritchard, Bragg Scattering Of Atoms From A Standing Light Wave, Phys. Rev. Lett. **60**, 515 (1988).
[34] P. H. Bucksbaum, D. W. Schumacher, and M. Bashkansky, High-Intensity Kapitza-Dirac Effect, Phys. Rev. Lett. **61**, 1182 (1988).
[35] D. L. Freimund, K. Aflatooni, and H. Batelaan, Observation of the Kapitza-Dirac effect, Nature (London) **413**, 142 (2001).
[36] D. L. Freimund and H. Batelaan, Bragg Scattering Of Free Electrons Using The Kapitza-Dirac Effect, Phys. Rev. Lett. **89**, 283602 (2002).
[37] H. Batelaan, The Kapitza-Dirac effect, Contemp. Phys. **41**, 369 (2000).
[38] H. Batelaan, Colloquium: Illuminating the Kapitza-Dirac effect with electron matter optics, Rev. Mod. Phys. **79**, 929 (2007).
[39] D. L. Freimund and H. Batelaan, A microscropic Stern-Gerlach magnet for electrons? Laser Phys. **13**, 892 (2003).
[40] L. Rosenberg, Extended theory of Kapitza-Dirac scattering, Phys. Rev. A **70**, 023401 (2004).
[41] S. Ahrens, H. Bauke, C. H. Keitel, and C. Müller, Spin Dynamics In The Kapitza-Dirac Effect, Phys. Rev. Lett. **109**, 043601 (2012).
[42] S. Ahrens, H. Bauke, C. H. Keitel, and C. Müller, Kapitza-dirac effect in the relativistic regime, Phys. Rev. A **88**, 012115 (2013).
[43] H. Bauke, S. Ahrens, C. H. Keitel, and R. Grobe, Electron-spin dynamics induced by photon spins, New J. Phys. **16**, 103028 (2014).
[44] H. Bauke, S. Ahrens, and R. Grobe, Electron-spin dynamics in elliptically polarized light waves, Phys. Rev. A **90**, 052101 (2014).
[45] R. Erhard and H. Bauke, Spin effects in Kapitza-Dirac scattering at light with elliptical polarization, Phys. Rev. A **92**, 042123 (2015).
[46] S. McGregor, W. C.-W. Huang, B. A. Shadwick, and H. Batelaan, Spin-dependent two-color Kapitza-Dirac effects, Phys. Rev. A **92**, 023834 (2015).
[47] M. M. Dellweg, H. M. Awwad, and C. Müller, Spin dynamics in Kapitza-Dirac scattering of electrons from bichromatic laser fields, Phys. Rev. A **94**, 022122 (2016).
[48] M. M. Dellweg and C. Müller, Spin-Polarizing Interferometric Beam Splitter For Free Electrons, Phys. Rev. Lett. **118**, 070403 (2017).
[49] M. M. Dellweg and C. Müller, Controlling electron spin dynamics in bichromatic Kapitza-Dirac scattering by the laser field polarization, Phys. Rev. A **95**, 042124 (2017).
[50] S. Ahrens, Electron-spin filter and polarizer in a standing light wave, Phys. Rev. A **96**, 052132 (2017).
[51] A. Ebadati, M. Vafaee, and B. Shokri, Four-photon Kapitza-Dirac effect as an electron spin filter, Phys. Rev. A **98**, 032505 (2018).
[52] A. Ebadati, M. Vafaee, and B. Shokri, Investigation of electron spin dynamic in the bichromatic Kapitza-Dirac effect via frequency ratio and amplitude of laser beams, Phys. Rev. A **100**, 052514 (2019).
[53] M. Kozák, Nonlinear inelastic scattering of electrons at an optical standing wave, Phys. Rev. A **98**, 013407 (2018).
[54] P. Panek, J. Z. Kamiński, and F. Ehlotzky, Laser-induced Compton scattering at relativistically high radiation powers, Phys. Rev. A **65**, 022712 (2002).
[55] D. Y. Ivanov, G. L. Kotkin, and V. G. Serbo, Complete description of polarization effects in emission of a photon by an electron in the field of a strong laser wave, Eur. Phys. J. C **36**, 127 (2004).
[56] M. Boca and V. Florescu, Nonlinear Compton scattering with a laser pulse, Phys. Rev. A **80**, 053403 (2009).
[57] K. Krajewska and J. Z. Kamiński, Spin effects in nonlinear Compton scattering in ultrashort linearly-polarized laser pulses, Laser Part. Beams **31**, 503 (2013).
[58] O. D. Skoromnik, I. D. Feranchuk, and C. H. Keitel, Collapse-and-revival dynamics of strongly laser-driven electrons, Phys. Rev. A **87**, 052107 (2013).
[59] B. King, Double Compton scattering in a constant crossed field, Phys. Rev. A **91**, 033415 (2015).
[60] D. Del Sorbo, D. Seipt, T. G. Blackburn, A. G. R. Thomas, C. D. Murphy, J. G. Kirk, and C. P. Ridgers, Spin polarization of electrons by ultraintense lasers, Phys. Rev. A **96**, 043407 (2017).
[61] D. Seipt, D. Del Sorbo, C. P. Ridgers, and A. G. R. Thomas, Theory of radiative electron polarization in strong laser fields, Phys. Rev. A **98**, 023417 (2018).
[62] Y.-F. Li, R. Shaisultanov, K. Z. Hatsagortsyan, F. Wan, C. H. Keitel, and J.-X. Li, Ultrarelativistic Electron-Beam Polarization In Single-Shot Interaction With An Ultraintense Laser Pulse, Phys. Rev. Lett. **122**, 154801 (2019).
[63] Y.-Y. Chen, P.-L. He, R. Shaisultanov, K. Z. Hatsagortsyan, and C. H. Keitel, Polarized Positron Beams Via Intense Two-Color Laser Pulses, Phys. Rev. Lett. **123**, 174801 (2019).
[64] M. Wen, M. Tamburini, and C. H. Keitel, Polarized Laser-WakeField-Accelerated Kiloampere Electron Beams, Phys. Rev. Lett. **122**, 214801 (2019).
[65] Y. Fu, Y. Liu, C. Wang, J. Zeng, and J. Yuan, Three-dimensional spin-dependent dynamics in linearly polarized standing-wave fields, Phys. Rev. A **100**, 013405 (2019).
[66] P. Kling, E. Giese, R. Endrich, P. Preiss, R. Sauerbrey, and W. P. Schleich, What defines the quantum regime of the free-electron laser? New J. Phys. **17**, 123019 (2015).
[67] P. Kling, R. Sauerbrey, P. Preiss, E. Giese, R. Endrich, and W. P. Schleich, Quantum regime of a free-electron laser: Relativistic approach, Appl. Phys. B **123**, 9 (2016).
[68] A. Debus, K. Steiniger, P. Kling, C. M. Carmesin, and R. Sauerbrey, Realizing quantum free-electron lasers: A critical analysis of experimental challenges and theoretical limits, Phys. Scr. **94**, 074001 (2019).
[69] P. Kling, E. Giese, C. M. Carmesin, R. Sauerbrey, and W. P. Schleich, High-gain quantum free-electron laser: Emergence and exponential gain, Phys. Rev. A **99**, 053823 (2019).
[70] C. M. Carmesin, P. Kling, E. Giese, R. Sauerbrey, and W. P. Schleich, Quantum and classical phase-space dynamics of a free-electron laser, Phys. Rev. Research **2**, 023027 (2020).
[71] S. Ahrens and C.-P. Sun, Spin in Compton scattering with pronounced polarization dynamics, Phys. Rev. A **96**, 063407 (2017).
[72] W. H. Furry, On bound states and scattering in positron theory, Phys. Rev. **81**, 115 (1951).

[73] V. B. Berestetskii, E. M. Lifshitz, and L. P. Pitaevskii, *Quantum Electrodynamics*, 2nd ed., Vol. 4 (Elsevier, Singapore, 1982).

[74] E. S. Fradkin, D. M. Gitman, and S. M. Shvartsman, *Quantum Electrodynamics with Unstable Vacuum* (Springer, New York, 1991).

[75] V. I. Ritus, Quantum effects of the interaction of elementary particles with an intense electromagnetic field, J. Sov. Laser Res. **6**, 497 (1985).

[76] F. Halzen and A. D. Martin, *Quarks and Leptons* (Wiley, New York, 1984).

[77] B. Shen, Z. Bu, J. Xu, T. Xu, L. Ji, R. Li, and Z. Xu, Exploring vacuum birefringence based on a 100 PW laser and an x-ray free electron laser beam, Plasma Phys. Control. Fusion **60**, 044002 (2018).

[78] M. Suzuki, Y. Inubushi, M. Yabashi, and T. Ishikawa, Polarization control of an x-ray free-electron laser with a diamond phase retarder, J. Synchrotron Radiat. **21**, 466 (2014).

[79] T. Osaka, M. Yabashi, Y. Sano, K. Tono, Y. Inubushi, T. Sato, S. Matsuyama, T. Ishikawa, and K. Yamauchi, A Bragg beam splitter for hard x-ray free-electron lasers, Opt. Express **21**, 2823 (2013).

[80] M. Kuwahara, S. Kusunoki, X. G. Jin, T. Nakanishi, Y. Takeda, K. Saitoh, T. Ujihara, H. Asano, and N. Tanaka, 30-kV spin-polarized transmission electron microscope with GaAs-GaAsP strained superlattice photocathode, Appl. Phys. Lett. **101**, 033102 (2012).

[81] https://lcls.slac.stanford.edu/. A. A. Lutman, M. W. Guetg, T. J. Maxwell, J. P. MacArthur, Y. Ding, C. Emma, J. Krzywinski, A. Marinelli, and Z. Huang, High-Power Femtosecond Soft X Rays from Fresh-Slice Multistage Free-Electron Lasers, Phys. Rev. Lett. **120**, 264801 (2018).

[82] https://www.xfel.eu/. *The European X-ray Free-electron Laser Technical Design Report*, edited by M. Altarelli, R. Brinkmann, M. Chergui, W. Decking, B. Dobson, S. Düsterer, G. Grübel, W. Graeff, H. Graafsma, J. Hajdu, J. Marangos, J. Pflüger, H. Redlin, D. Riley, I. Robinson, J. Rossbach, A. Schwarz, K. Tiedtke, T. Tschentscher, I. Vartaniants, H. Wabnitz, H. Weise, R. Wichmann, K. Witte, A. Wolf, M. Wulff, and M. Yurkov (DESY XFEL Project Group European XFEL Project Team Deutsches Elektronen-Synchrotron Member of the Helmholtz Association, Hamburg, 2007).

[83] Y. Salamin, Fields of a Gaussian beam beyond the paraxial approximation, Appl. Phys. B **86**, 319 (2006).

[84] G. R. Mocken and C. H. Keitel, Radiation spectra of laser-driven quantum relativistic electrons, Comput. Phys. Commun. **166**, 171 (2005).

[85] S. Ahrens, Investigation of the Kapitza-Dirac effect in the relativistic regime, Ph.D. thesis, Ruprecht-Karls University Heidelberg, 2012, http://archiv.ub.uni-heidelberg.de/volltextserver/14049/.

[86] M. E. Peskin and D. V. Schroeder, *An Introduction to Quantum Field Theory* (Beijing World Publishing Corp., 1995).

[87] L. H. Ryder, *Quantum Field Theory*, 2nd ed. (Cambridge University Press, Cambridge, 1986).

[88] M. Srednicki, *Quantum Field Theory*, 1st ed. (Cambridge University Press, Cambridge, 2007).

[89] F. Schwabl, *Advanced Quantum Mechanics* (Springer, New York, 2000).